FADD and caspase-8 regulate gut homeostasis and inflammation by controlling MLKL- and GSDMD-mediated death of intestinal epithelial cells

Robin Schwarzer[1,2], Huipeng Jiao[1,2], Laurens Wachsmuth[1,2], Achim Tresch[2,3,4] & Manolis Pasparakis[1,2,5,6,*]

[1]Institute for Genetics, University of Cologne, 50674 Cologne, Germany
[2]Cologne Excellence Cluster on Cellular Stress Responses in Aging-Associated Diseases (CECAD), University of Cologne, 50931 Cologne, Germany
[3]Institute of Medical Statistics and Computational Biology, Faculty of Medicine, University of Cologne, Bachemer Str. 86, 50931, Cologne, Germany.
[4]Center for Data and Simulation Science (CDS), University of Cologne, Cologne, Germany.
[5]Center for Molecular Medicine (CMMC), University of Cologne, 50931 Cologne, Germany

[6]Lead contact

*Correspondence: pasparakis@uni-koeln.de

Summary

Pathways controlling intestinal epithelial cell (IEC) death regulate gut immune homeostasis and contribute to the pathogenesis of inflammatory bowel diseases. Here we show that caspase-8 and its adapter FADD act in IECs to regulate intestinal inflammation downstream of Z-DNA binding protein 1 (ZBP1)- and tumor necrosis factor receptor-1 (TNFR1)-mediated receptor interacting protein kinase 1 (RIPK1) and RIPK3 signaling. Mice with IEC-specific FADD or caspase-8 deficiency developed colitis dependent on mixed lineage kinase-like (MLKL)-mediated epithelial cell necroptosis. However, MLKL deficiency fully prevented ileitis caused by epithelial caspase-8 ablation, but only partially ameliorated ileitis in mice lacking FADD in IECs. Our genetic studies revealed that caspase-8 and gasdermin-D (GSDMD) were both required for the development of MLKL-independent ileitis in mice with epithelial FADD deficiency. Therefore, FADD prevents intestinal inflammation downstream of ZBP1 and TNFR1 by inhibiting both MLKL-induced necroptosis and caspase-8-GSDMD-dependent pyroptosis-like death of epithelial cells.

Introduction

The intestinal epithelium plays an important role for the maintenance of gut immune homeostasis by forming a physical and chemical barrier separating luminal microbes and mucosal immune cells (Turner, 2009). Impaired epithelial barrier function has been reported in patients presenting with inflammatory bowel disease (IBD) and their healthy first-degree relatives, thus identifying epithelial permeability defects as possible causal factors in IBD (Buhner et al., 2006; Katz et al., 1989; Kiesslich et al., 2012; Turner, 2009). Therefore, mechanisms regulating the survival and death of IECs are critical for immune homeostasis and the pathogenesis of inflammatory diseases in the gut. Indeed, studies in genetic mouse models provide evidence that death of IECs triggers severe chronic inflammatory pathologies (Dannappel et al., 2014; Eftychi et al., 2019; Gunther et al., 2011; Nenci et al., 2007; Takahashi et al., 2014; Vlantis et al., 2016; Welz et al., 2011).

Fas associated with death domain (FADD) is an adapter essential for caspase-8 activation downstream of death receptors (Chinnaiyan et al., 1996; Muzio et al., 1996). FADD-mediated activation of caspase-8 is essential for death receptor-induced apoptosis, but also for inhibiting receptor interacting protein kinase 3 (RIPK3)-MLKL-dependent necroptosis, as shown by the rescue of the embryonic lethality of *Fadd*^{-/-} or *Casp8*^{-/-} mice by crossing to *Ripk3*^{-/-} or *Mlkl*^{-/-} animals (Alvarez-Diaz et al., 2016; Kaiser et al., 2011; Oberst et al., 2011; Zhang et al., 2011). Mice lacking FADD in IECs (*Fadd*^{fl/fl} x *Vil1*-cre, *Fadd*[IEC-KO]) develop chronic inflammatory colitis and ileitis accompanied with pronounced loss of Paneth cells, specialized anti-microbial peptide-producing secretory cells of the intestinal crypt (Welz et al., 2011). Mice with IEC-

specific caspase-8 deficiency (*Casp8fl/fl x Vil1-cre, Casp8*[IEC-KO]) have been reported to develop ileitis with loss of Paneth cells (Gunther et al., 2011), as well as colitis depending on the microbiota (Stolzer et al., 2020). Ubiquitous RIPK3 deficiency prevents colitis and ileitis in *Fadd*[IEC-KO] mice, suggesting that epithelial cell necroptosis drives the pathology in both the small and large intestine (Welz et al., 2011). Consistently, RIPK3 deficiency prevents ileitis in *Casp8*[IEC-KO] mice (Wittkopf et al., 2013) as well as intestinal inflammation caused by inducible caspase-8 ablation (Weinlich et al., 2013). Together, these studies support that epithelial FADD or caspase-8 deficiencies cause intestinal inflammation by sensitizing IECs to RIPK3-dependent necroptosis. However, in addition to inducing MLKL-dependent necroptosis, RIPK3 can also trigger FADD-caspase-8-mediated apoptosis, and is implicated in cell death-independent functions including inflammatory cytokine production in mucosal dendritic cells as well as inflammasome regulation (Lawlor et al., 2015; Moriwaki et al., 2017; Moriwaki et al., 2014). Therefore, the mechanisms driving intestinal inflammation in *Fadd*[IEC-KO] and *Casp8*[IEC-KO] mice and particularly the contribution of MLKL-dependent necroptosis have remained unclear. TNF deficiency strongly inhibits colitis in *Fadd*[IEC-KO] mice (Welz et al., 2011), suggesting that TNF critically contributes to colon inflammation likely by inducing RIPK3-MLKL-dependent IEC necroptosis. However, TNF or TNFR1 deficiency does not prevent ileitis in *Fadd*[IEC-KO] (Welz et al., 2011) or *Casp8*[IEC-KO] mice (Wittkopf et al., 2013) respectively, suggesting that ileitis and Paneth cell loss caused by IEC-specific FADD or caspase-8 deficiency is driven by TNF-TNFR1-independent pathways that have remained elusive.

Here, we have shown that Z-DNA binding protein 1 (ZBP1, also known as DAI or DLM1) acted together with TNFR1 to trigger both colitis and ileitis in *Fadd*[IEC-KO] mice. Whereas colitis pathogenesis depended on MLKL-mediated necroptosis, ileitis development in *Fadd*[IEC-KO] mice was induced by both MLKL-dependent necroptosis and caspase-8-dependent activation of Gasdermin-D (GSDMD)-mediated pyroptosis of FADD-deficient IECs.

Results

Mice lacking FADD or caspase-8 in IECs develop colitis and ileitis
To study the role of FADD and caspase-8 in intestinal inflammation, we analyzed side by side *Fadd*[IEC-KO] and *Casp8*[IEC-KO] mice. As shown previously (Welz et al., 2011), *Fadd*[IEC-KO] mice develop spontaneous colitis characterized by death of IECs, epithelial erosion and hyperplasia, as well as increased infiltration of CD45^{+} immune cells in the mucosa and/or submucosa (Figures 1A and 1B). Colitis severity varied between individual mice, with about 60% of the animals developing ulcers that were usually found in the middle section of the colon (Figure 1C and data not shown). *Casp8*[IEC-KO] mice also developed spontaneous colitis although the pathology was overall less severe compared to *Fadd*[IEC-KO] mice (Figures 1A-C). Microarray profiling revealed gene expression changes characteristic of pronounced inflammation in the colons of *Fadd*[IEC-KO] and *Casp8*[IEC-KO] mice, with the latter showing an overall milder phenotype consistent with the histological analysis (Figure 1D). Inflammatory signature genes were amongst the most notably induced genes in both genotypes (Figure 1E and 1F).

In line with previous reports (Gunther et al., 2011; Welz et al., 2011), *Fadd*[IEC-KO] and *Casp8*[IEC-KO] mice showed loss of Paneth cells in the ileum, revealed by strongly reduced numbers of lysozyme^{+} cells and decreased mRNA expression of Paneth cell-associated genes including *Ang4*, *Lyz1* and *Defa-rs2* (Figure S1A-B). Furthermore, both *Fadd*[IEC-KO] and *Casp8*[IEC-KO] mice spontaneously developed ileitis characterized by epithelial hyperplasia, IEC death, increased immune cell infiltration in the lamina propria, as well as altered gene expression profiles indicative of intestinal inflammation (Figure S1C-F). As in colitis, ileitis in *Fadd*[IEC-KO] mice was more severe compared to *Casp8*[IEC-KO] (Figure S1E-F), indicating that FADD deficiency elicits additional responses compared to loss of caspase-8 that contribute to intestinal tissue pathology.

TNFR1 and ZBP1 promote colitis development in $Fadd^{IEC-KO}$ mice

Ubiquitous TNF deficiency prevents colitis in $Fadd^{IEC-KO}$ mice (Welz et al., 2011), suggesting that TNF may cause the disease by triggering necroptosis of FADD-deficient IECs. To address the epithelial cell intrinsic role of TNFR1, we generated and analyzed $Fadd^{fl/fl}$ x $Tnfr1^{fl/fl}$ x $Vil1$-cre ($Fadd^{IEC-KO}$ $Tnfr1^{IEC-KO}$) and $Casp8^{fl/fl}$ x $Tnfr1^{fl/fl}$ x $Vil1$-cre ($Casp8^{IEC-KO}$ $Tnfr1^{IEC-KO}$) mice. Consistent with elevated TNF expression, IEC-specific ablation of TNFR1 strongly inhibited colitis development and prevented ulcer formation in both $Fadd^{IEC-KO}$ and $Casp8^{IEC-KO}$ mice (Figure 2A-C and S2A-D). However, both $Casp8^{IEC-KO}$ $Tnfr1^{IEC-KO}$ and $Fadd^{IEC-KO}$ $Tnfr1^{IEC-KO}$ mice showed focal mild immune cell infiltration in the colon at the age of 10-12 weeks (Figure 2A-B and S2B-C), suggesting that, although TNFR1 plays a major role in driving colitis development, TNFR1-independent mechanisms may also be involved. Indeed, analysis of mice at the age of 7-12 months revealed that about half of the $Fadd^{IEC-KO}$ $Tnfr1^{IEC-KO}$ mice developed mild colon inflammation, which was however less severe compared to the lesions observed in young $Fadd^{IEC-KO}$ mice (Figure 2A-C). Similar to epithelial TNFR1 deficiency, inhibition of RIPK1 kinase activity by crossing with $Ripk1^{D138N/D138N}$ mice expressing kinase inactive RIPK1 (Polykratis et al., 2014) strongly suppressed colitis development in both models (Figure S2E-G). However, some $Fadd^{IEC-KO}$ $Ripk1^{D138N/D138N}$ mice developed colon inflammation later in life (Dannappel et al., 2014), suggesting that also RIPK1-independent mechanisms are involved. Thus, TNFR1-RIPK1 signaling plays an important role but also TNFR1-RIPK1-independent mechanisms contribute to the pathogenesis of colitis in $Fadd^{IEC-KO}$ and $Casp8^{IEC-KO}$ mice.

In an effort to elucidate the TNF-independent mechanisms driving colitis in $Fadd^{IEC-KO}$ mice, we compared microarray gene expression profiles with histological colitis scores within individual mice to identify genes the expression of which correlated best with disease severity. Among the top 25 genes for which increased expression correlated with increased colitis severity, we identified the gene encoding ZBP1 (Figure S2H). Increased expression of ZBP1 protein in colonic IECs of $Fadd^{IEC-KO}$ mice was confirmed by immunoblotting (Figure S2I). ZBP1 activates RIPK3 in a RIP homotypic interaction motif (RHIM)-dependent manner and has been shown to trigger RIPK3-dependent cell death and inflammation in response to infection with certain viruses but also in the skin of mice lacking RIPK1 or expressing RIPK1 with mutated RHIM (Kuriakose et al., 2016; Lin et al., 2016; Newton et al., 2016b; Nogusa et al., 2016; Upton et al., 2012). We therefore postulated that ZBP1 may contribute to RIPK3-mediated epithelial cell death and intestinal inflammation in $Fadd^{IEC-KO}$ mice. Indeed, histological assessment and microarray gene expression profiling of colon tissue from $Fadd^{IEC-KO}$ $Zbp1^{-/-}$ mice at the age of 10-12 weeks revealed that ZBP1 deficiency strongly inhibited colitis development (Figure 2D-G). However, similarly to $Fadd^{IEC-KO}$ $Tnfr1^{IEC-KO}$ mice, histological examination of colon tissue from 9-10 month old $Fadd^{IEC-KO}$ $Zbp1^{-/-}$ mice revealed low grade inflammatory lesions (Figure 2D-F). Collectively, these results identified ZBP1, in addition to TNFR1, as a critical factor that drives colitis development in $Fadd^{IEC-KO}$ mice.

TNFR1 and ZBP1 act redundantly to cause ileitis in $Fadd^{IEC-KO}$ mice

Having established TNFR1 and ZBP1 as major drivers of colitis in $Fadd^{IEC-KO}$ mice, we wondered whether they also contribute to the pathogenesis of ileitis. Consistent with earlier results in $Fadd^{IEC-KO}$ $Tnf^{-/-}$ mice (Welz et al., 2011), IEC-specific TNFR1 ablation did not considerably suppress ileitis in $Fadd^{IEC-KO}$ mice, although a slight trend towards reduced severity was noted (Figure 3A-B). In contrast to a previous study suggesting a critical role for TNFR1 (Gunther et al., 2011), IEC-specific TNFR1 deficiency did not prevent ileitis development and Paneth cell loss in $Casp8^{IEC-KO}$ mice (Figure S3A-B).

Histological assessment and microarray gene expression analysis of small intestinal tissue revealed that ablation of ZBP1 did not considerably prevent ileitis in $Fadd^{IEC-KO}$ mice, although $Fadd^{IEC-KO}$ $Zbp1^{-/-}$ mice showed a mild overall amelioration of the pathology (Figure 3A-C). Intrigued by the similar effect of ZBP1 or TNFR1 deficiencies in mildly ameliorating ileitis in $Fadd^{IEC-KO}$ mice, we wondered whether the two pathways might exhibit functional redundancy. Indeed, histological examination of intestinal sections from $Fadd^{IEC-KO}$ $Tnfr1^{IEC-KO}$ $Zbp1^{-/-}$ mice

revealed that combined deficiency of TNFR1 and ZBP1 strongly ameliorated - but did not fully prevent - ileitis development, as shown by overall restored tissue architecture, reduced numbers of dying IECs, partial re-appearance of Paneth cells and reduced CD45$^+$ immune cell infiltrates (Figure 3A-B, D). The redundant role of TNFR1 and ZBP1 in driving ileitis as opposed to their synergistic effect in driving colitis could be related to their increased expression in the ileum compared to the colon (Figure S3F and S2I). We hypothesized that TIR domain-containing adapter protein inducing IFN-beta (TRIF, also known as TICAM-1), an adapter protein mediating signaling downstream of TLR3 and TLR4 that contains a RHIM and can activate RIPK3 (Pasparakis and Vandenabeele, 2015), might also contribute to the pathology, therefore we generated and analyzed $Fadd^{fl/fl}$ x $Tnfr1^{fl/fl}$ x $Ticam1^{fl/fl}$ x $Vil1$-cre x $Zbp1^{-/-}$ mice ($Fadd^{IEC-KO}$ $Tnfr1^{IEC-KO}$ $Ticam1^{IEC-KO}$ $Zbp1^{-/-}$). Additional epithelial ablation of TRIF fully restored the numbers of lysozyme$^+$ Paneth cells (Figure 3B), but could not fully prevent ileitis as these mice still showed mild epithelial hyperplasia and small numbers of dying epithelial cells (Figure 3A, 3B and 3E). Notably, ablation of TRIF did not show any additive effect when combined with TNFR1 deficiency in the presence of $Zbp1$ heterozygosity (Figure 3A). Collectively, these results revealed that TNFR1 and ZBP1 act in a redundant fashion to induce IEC death and ileitis development in $Fadd^{IEC-KO}$ mice, while TRIF also contributes particularly to the loss of Paneth cells.

Inhibition of RIPK1 kinase activity strongly suppressed ileitis development in both $Fadd^{IEC-KO}$ $Ripk1^{D138N/D138N}$ and $Casp8^{IEC-KO}$ $Ripk1^{D138N/D138N}$ mice (Figure S3C-E). The kinase inactive $Ripk1^{D138N/D138N}$ had a similar effect in suppressing ileitis compared to combined TNFR1+ZBP1 deficiency (Figure S3C and S3E), suggesting that RIPK1 acts downstream of both receptors. Considering that RIPK1 has been shown to inhibit ZBP1-mediated necroptosis and inflammation in the skin (Lin et al., 2016; Newton et al., 2016b), we explored the role of RIPK1 in ZBP1-mediated cell death in cellular systems. Doxycycline-inducible expression of ZBP1 in mouse embryonic fibroblasts (MEFs) caused cell death in the presence, but not in the absence, of the caspase inhibitor emricasan, which was strongly inhibited by the RIPK1-specific inhibitor necrostatin-1s (Nec-1s) (Figure 3F, G). To assess whether endogenous ZBP1 also mediates RIPK1-dependent cell death, we employed primary lung fibroblasts (LFs). Emricasan treatment induced cell death in WT LFs, that was strongly, but not completely, suppressed in $Tnfr1^{-/-}$ LFs, suggesting that this is induced by autocrine TNF signaling (Figure 3H). Emricasan-induced cell death was only partially inhibited in $Zbp1^{-/-}$ LFs, but was fully prevented by combined deficiency of TNFR1 and ZBP1 (Figure 3H). We reasoned that the minor role of ZBP1 in this setting might be due to its very low expression and repeated the experiment in cells that were prestimulated with IFNγ for 24 hours to induce ZBP1 expression (Figure 3I). LFs lacking both TNFR1 and ZBP1 were fully protected by IFNγ+emricasan-induced cell death, whereas single TNFR1 or ZBP1 deficiencies offered little protection (Figure 3H), demonstrating that ZBP1 and TNFR1 exhibit redundant functions in driving IFNγ+emricasan-induced cell death, in line with our findings that ZBP1 and TNFR1 act redundantly to induce ileitis in $Fadd^{IEC-KO}$ mice. Furthermore, LFs from $Ripk1^{D138N/D138N}$ mice were considerably protected from IFNγ+emricasan-induced death, showing that RIPK1 kinase activity drives cell death downstream of TNFR1 and ZBP1 (Figure 3H). Consistently, IFNγ+emricasan treatment caused phosphorylation of RIPK1 and MLKL that were abolished in $Tnfr1^{-/-}$ $Zbp1^{-/-}$ LFs (Figure 3I and 3J). Moreover, Nec-1s treatment inhibited phosphorylation of MLKL in IFNγ+emricasan treated $Tnfr1^{-/-}$ LFs, demonstrating that ZBP1-mediated necroptosis required RIPK1 kinase activity (Figure 3I and 3J). Together, these results showed that TNFR1 and ZBP1 act redundantly to induce necroptosis and intestinal inflammation when FADD-caspase-8 signaling is impaired.

MLKL-dependent and -independent mechanisms cause ileitis in $Fadd^{IEC-KO}$ mice
Ubiquitous RIPK3 deficiency prevents colitis and ileitis in $Fadd^{IEC-KO}$ mice (Welz et al., 2011) suggesting that necroptosis of $Fadd$-deficient IECs causes intestinal inflammation. However, since RIPK3 has been reported to regulate intestinal inflammation by acting on immune cells independently from necroptosis (Moriwaki et al., 2014), to address the role of epithelial RIPK3 we generated $Fadd^{fl/fl}$ x $Ripk3^{fl/fl}$ x $Vil1$-cre mice ($Fadd^{IEC-KO}$ $Ripk3^{IEC-KO}$). IEC-specific RIPK3 ablation prevented colitis development in $Fadd^{IEC-KO}$ mice, as shown by histological and gene

expression analysis (Figure 4A-E). To exclude the involvement of non-necroptotic functions of RIPK3 and unequivocally assess the contribution of necroptosis in colitis development, we generated and analyzed $Fadd^{IEC-KO}$ $Mlkl^{-/-}$ as well as $Casp8^{IEC-KO}$ $Mlkl^{-/-}$ mice (Figure 4F). Indeed, histological analysis and microarray gene expression profiling revealed that MLKL deficiency prevented colitis development in $Fadd^{IEC-KO}$ and $Casp8^{IEC-KO}$ mice (Figure 4G-J). Taken together, these results showed that RIPK3-MLKL-dependent IEC necroptosis causes colitis in $Fadd^{IEC-KO}$ and $Casp8^{IEC-KO}$ mice.

Histological analysis of ileal sections from $Fadd^{IEC-KO}$ $Ripk3^{IEC-KO}$ mice revealed that IEC-specific RIPK3 deletion strongly suppressed epithelial hyperplasia, cell death and tissue inflammation, and largely restored the appearance of lysozyme$^+$ Paneth cells in $Fadd^{IEC-KO}$ mice (Figure 5A-B). However, mild epithelial hyperplasia, small numbers of dying IECs as well as mildly decreased Paneth cell numbers were observed in $Fadd^{IEC-KO}$ $Ripk3^{IEC-KO}$ mice (Figure 5A-C). Furthermore, microarray profiling revealed that RIPK3 epithelial deficiency largely restored but did not completely normalize gene expression in the ileum of $Fadd^{IEC-KO}$ mice (Figure 5D). Therefore, IEC-specific RIPK3 deficiency strongly inhibited but did not completely prevent ileitis in $Fadd^{IEC-KO}$ mice. To unequivocally assess the role of necroptosis in ileitis development we analyzed ileal tissues from $Casp8^{IEC-KO}$ $Mlkl^{-/-}$ and $Fadd^{IEC-KO}$ $Mlkl^{-/-}$ mice. MLKL deficiency fully prevented the development of ileal pathology in $Casp8^{IEC-KO}$ mice, as assessed by immunohistological and gene expression analysis (Figure 5E-H), demonstrating that MLKL-dependent IEC necroptosis causes ileitis in these animals. In contrast, analysis of $Fadd^{IEC-KO}$ $Mlkl^{-/-}$ mice revealed that MLKL-deficiency only partially inhibited ileitis in $Fadd^{IEC-KO}$ mice. Examination of ileal tissues from $Fadd^{IEC-KO}$ $Mlkl^{-/-}$ mice revealed increased cellularity in the mucosa, crypt hyperplasia, dying IECs, increased CD45$^+$ cell infiltration and decreased number of Paneth cells compared to $Fadd^{fl/fl}$ $Mlkl^{-/-}$ littermates (Figure 5E-G). Moreover, microarray analysis showed that the gene expression profiles of $Fadd^{IEC-KO}$ $Mlkl^{-/-}$ mice were more similar to $Casp8^{IEC-KO}$ and $Fadd^{IEC-KO}$ mice than to the floxed control mice (Figure 5H). Collectively, these results showed that epithelial caspase-8 deficiency causes ileitis by sensitizing IECs to MLKL-dependent necroptosis, but epithelial FADD deficiency causes ileitis by triggering MLKL-dependent necroptosis and by additional MLKL-independent mechanisms.

Caspase-8 drives MLKL-independent ileitis in $Fadd^{IEC-KO}$ mice

To explore the mechanisms causing MLKL-independent ileitis we examined intestinal sections from $Fadd^{IEC-KO}$ $Mlkl^{-/-}$ mice for signs of cell death by immunohistochemical staining for activated cleaved caspase-3 (CC3). Indeed, increased numbers of CC3$^+$ cells were detected in the small intestinal epithelium of $Fadd^{IEC-KO}$ $Mlkl^{-/-}$ but not in $Casp8^{IEC-KO}$ $Mlkl^{-/-}$ mice (Figure 6A). Increased numbers of cleaved caspase-8$^+$ (CC8$^+$) cells were also detected primarily in ileal crypts of $Fadd^{IEC-KO}$ and $Fadd^{IEC-KO}$ $Mlkl^{-/-}$ mice (Figure 6B). Prompted by the presence of CC8$^+$ IECs in $Fadd^{IEC-KO}$ $Mlkl^{-/-}$ mice combined with the fact that MLKL deficiency fully prevented ileitis in $Casp8^{IEC-KO}$ mice, we hypothesized that caspase-8 might trigger IEC death and ileitis in $Fadd^{IEC-KO}$ $Mlkl^{-/-}$ mice. Hence, we generated and analyzed $Fadd^{IEC-KO}$ $Casp8^{IEC-KO}$ $Mlkl^{-/-}$ mice. Indeed, additional IEC-specific deletion of caspase-8 fully prevented the small intestinal pathology observed in $Fadd^{IEC-KO}$ $Mlkl^{-/-}$ mice, as shown by normal tissue architecture with absence of infiltrating CD45$^+$ mucosal immune cells and CC3$^+$ IECs, as well as restored numbers of Lysozyme+ Paneth cells (Figure 6A and 6C-E). In agreement with the histological assessment, microarray analysis revealed that the ileal gene expression profile of $Fadd^{IEC-KO}$ $Casp8^{IEC-KO}$ $Mlkl^{-/-}$ mice clustered in close proximity to $Casp8^{IEC-KO}$ $Mlkl^{-/-}$ and $Fadd^{fl/fl}$ mice (Figure 6F). We then wondered whether caspase-8 contributed to ileitis development in $Fadd^{IEC-KO}$ mice also in the presence of MLKL. Indeed, analysis of intestinal tissues from $Fadd^{IEC-KO}$ $Casp8^{IEC-KO}$ mice revealed mildly decreased tissue inflammation and epithelial hyperplasia compared to $Fadd^{IEC-KO}$ mice, with an overall histological pathology score similar to that of $Casp8^{IEC-KO}$ mice (Figure 6G-I). Moreover, the expression of $Il1b$, $Il6$ and $Ccl2$ mRNAs was decreased in the ileum of $Fadd^{IEC-KO}$ $Casp8^{IEC-KO}$ compared to $Fadd^{IEC-KO}$ mice, further supporting that caspase-8 deficiency reduced inflammation (Figure 6J). Analysis of the mRNA expression of Paneth cell specific marker genes also supported the partial restoration of

Paneth cells in *Fadd*[IEC-KO] *Casp8*[IEC-KO] mice (Figure 6K). Together, these results showed that caspase-8 promotes ileitis in *Fadd*[IEC-KO] mice both in the absence and in the presence of MLKL.

Our genetic studies showing that caspase-8 triggers MLKL-independent ileitis in *Fadd*[IEC-KO] mice raised the question how is caspase-8 activated in the absence of its bona-fide adapter FADD. To gain insight into possible upstream pathways regulating caspase-8, we examined caspase-8 activation by immunostaining for CC8 in the ileum of the different genetic lines crossed to *Fadd*[IEC-KO] mice. Similar numbers of intestinal crypts containing CC8+ cells were detected in ileal sections from *Fadd*[IEC-KO] *Tnfr1*[IEC-KO] compared to *Fadd*[IEC-KO] mice, while *Fadd*[IEC-KO] *Zbp1*^{-/-} and *Fadd*[IEC-KO] *Tnfr1*[IEC-KO] *Zbp1*^{-/-} had mildly decreased numbers of CC8+ crypts (Figure S4A and S4B). Moreover, neither deletion of ZBP1 nor inhibition of RIPK1 kinase activity could suppress ileitis and the appearance of CC8+ crypts in *Fadd*[IEC-KO] *Mlkl*^{-/-} mice (Figure S4A-D). However, considerably reduced numbers of CC8+ crypts were detected in *Fadd*[IEC-KO] *Ripk3*[IEC-KO] and *Fadd*[IEC-KO] *Tnfr1*[IEC-KO] *Zbp1*^{-/-} *Ticam1*[IEC-KO] samples (Figure S4A and S4B), consistent with the overall stronger protection of these mouse strains from ileal tissue pathology (see Figure 3, Figure 5 and Table S1). Taken together, these results showed that TNFR1, ZBP1 and TRIF redundantly contribute to triggering RIPK3-mediated activation of caspase-8 in IECs from *Fadd*[IEC-KO] mice. However, a small number of CC8+ cells were still detected even in *Fadd*[IEC-KO] *Ripk3*[IEC-KO] and *Fadd*[IEC-KO] *Tnfr1*[IEC-KO] *Zbp1*^{-/-} *Ticam1*[IEC-KO] mice, suggesting that while this pathway clearly contributes to caspase-8 activation, also other pathways are involved in activating caspase-8 to a lesser extent. Apoptosis-associated speck-like protein containing a CARD (ASC) has been reported to associate with caspase-8 through PYRIN domain (PYD)-death effector domain (DED)-dependent heterotypic interactions (Masumoto et al., 2003; Sagulenko et al., 2013), and activate caspase-8-dependent cell death downstream of inflammasome receptors (Lee et al., 2018; Man et al., 2013; Mascarenhas et al., 2017; Pierini et al., 2012; Rauch et al., 2017; Sagulenko et al., 2013). We therefore hypothesized that ASC-dependent signals could activate caspase-8 in FADD-deficient IECs. Upon activation, ASC forms speck-like structures that act as platforms for the activation of downstream mediators. Immunostaining of small intestinal sections with an ASC-specific antibody revealed the presence of ASC specks in the epithelium of *Fadd*[IEC-KO] *Mlkl*^{-/-} but not *Mlkl*^{-/-} mice (Figure S5A), indicating that ASC might be involved in driving caspase-8 activation in these mice. However, IEC-specific ASC ablation did not prevent IEC death and the development of ileitis in *Fadd*[IEC-KO] or *Fadd*[IEC-KO] *Mlkl*^{-/-} mice (Figure S5B-F), showing that ASC is not essential for activation of caspase-8 in FADD-deficient IECs and the development of MLKL-independent intestinal inflammation.

Caspase-8 triggers GSDMD-dependent ileitis in *Fadd*[IEC-KO] *Mlkl*^{-/-} mice

The presence of increased numbers of CC8+ and CC3+ cells in *Fadd*[IEC-KO] *Mlkl*^{-/-} but not in *Fadd*[IEC-KO] *Casp8*[IEC-KO] *Mlkl*^{-/-} mice suggested that caspase-8 may cause ileitis by inducing apoptosis of IECs. However, caspase-8 was recently reported to also mediate Gasdermin-D (GSDMD)-dependent cell death (Orning et al., 2018; Sarhan et al., 2018). Considering that apoptosis is generally believed not to cause inflammation while GSDMD triggers inflammatory lytic cell death, we hypothesized that caspase-8 might trigger ileitis in *Fadd*[IEC-KO] *Mlkl*^{-/-} mice by activating GSDMD. To address the role of GSDMD, we generated *Fadd*[IEC-KO] *Mlkl*^{-/-} *Gsdmd*^{-/-} mice using CRISPR-Cas9-mediated targeting of the *Gsdmd* gene in fertilized oocytes from *Fadd*[IEC-KO] *Mlkl*^{-/-} mice. The obtained F0 generation was intercrossed and mice from the F1 generation were analyzed for ileitis development (Figure 7A). To confirm GSDMD deficiency, we assessed the expression of GSDMD protein in spleen protein extracts from all F1 mice that were analyzed for intestinal pathology (Figure 7B). *Fadd*[IEC-KO] *Mlkl*^{-/-} *Gsdmd*^{-/-} mice showed restored tissue architecture, re-appearance of Lysozyme+ Paneth cells and absence of infiltrating immune cells, showing that GSDMD deficiency inhibited ileitis development in *Fadd*[IEC-KO] *Mlkl*^{-/-} mice (Figure 7C and 7D and Table S1). However, CC8+ and CC3+ cells were still detected in small intestinal crypts from *Fadd*[IEC-KO] *Mlkl*^{-/-} *Gsdmd*^{-/-} mice, suggesting that, in the absence of GSDMD, caspase-8 triggers caspase-3-dependent apoptosis of FADD-deficient IECs, which however is not sufficient to cause ileitis (Figure 7E, 7F, 7G). Taken

together, these results showed that caspase-8 promotes ileal inflammation in $Fadd^{IEC-KO}$ $Mlkl^{-/-}$ mice by inducing GSDMD-dependent death of IECs.

Discussion

Earlier studies suggested that RIPK3-dependent IEC necroptosis causes colitis and ileitis in mice lacking FADD or caspase-8 in the intestinal epithelium (Weinlich et al., 2013; Welz et al., 2011; Wittkopf et al., 2013). Indeed, our results confirmed that MLKL-dependent necroptosis of IECs causes colitis and ileitis in $Casp8^{IEC-KO}$ mice. Considering that the only function known for FADD is to act as an adapter facilitating the activation of caspase-8, it was therefore unexpected that MLKL deficiency rescued colitis but only partially ameliorated ileitis development in $Fadd^{IEC-KO}$ mice. Our genetic experiments demonstrating that caspase-8 causes MLKL-independent ileitis in $Fadd^{IEC-KO}$ mice, revealed not only that activation of caspase-8 in this context does not require FADD but on the contrary it is inhibited by FADD. The detection of IECs staining positive for CC3 and CC8 in $Fadd^{IEC-KO}$ $Mlkl^{-/-}$ mice suggested that caspase-8 could trigger ileitis by inducing epithelial cell apoptosis. However, taking into account that apoptosis is generally considered a non-inflammatory type of cell death (Pasparakis and Vandenabeele, 2015), we explored an alternative hypothesis. Based on recent studies showing that caspase-8 could induce activation of GSDMD-dependent pyroptosis (Orning et al., 2018; Sarhan et al., 2018), we hypothesized that caspase-8 may activate GSDMD-dependent cell death in IECs of $Fadd^{IEC-KO}$ $Mlkl^{-/-}$ mice triggering inflammation. Indeed, our genetic studies showing that GSDMD deficiency inhibited ileitis in $Fadd^{IEC-KO}$ $Mlkl^{-/-}$ mice provided experimental evidence supporting that caspase-8-dependent activation of GSDMD drives the pathology. Nevertheless, CC3$^+$ and CC8$^+$ epithelial cells could still be detected in $Fadd^{IEC-KO}$ $Mlkl^{-/-}$ $Gsdmd^{-/-}$ mice, suggesting that, in the absence of GSDMD, caspase-8 triggers caspase-3-dependent apoptosis, which is however not sufficient to trigger inflammation. This finding is consistent with the generally accepted notion that apoptotic cell death is immunologically silent in contrast to the highly inflammatory nature of lytic cell death such as necroptosis or pyroptosis (Pasparakis and Vandenabeele, 2015). Therefore, our data provide *in vivo* experimental evidence that activation of caspase-8 can trigger both non-inflammatory apoptosis but also inflammatory lytic cell death in IECs depending on the downstream effectors that are activated to induce cell death execution.

While it remains to be experimentally assessed whether GSDMD deficiency also ameliorates ileitis in $Fadd^{IEC-KO}$ mice in the presence of MLKL, our results showing that caspase-8 deficiency ameliorated ileitis in $Fadd^{IEC-KO}$ mice suggest that the caspase-8-GSDMD-dependent axis also operates in the presence of MLKL. It is currently unclear whether caspase-8 induces GSDMD activation in $Fadd^{IEC-KO}$ $Mlkl^{-/-}$ IECs by direct proteolytic processing or indirectly, e.g. via caspases 1 and 11. However, the finding that ASC deficiency could not prevent ileitis in $Fadd^{IEC-KO}$ $Mlkl^{-/-}$ mice argues against an indirect activation of GSDMD by caspase-8 through ASC-caspase-1. Two recent studies report that catalytically inactive caspase-8 induces MLKL-independent, ASC-caspase-1-dependent intestinal pathology and perinatal lethality in mice (Fritsch et al., 2019; Newton et al., 2019). These results suggest that caspase-8 acts as a scaffold to activate the ASC-caspase-1 inflammasome and that caspase-8 catalytic activity prevents inflammasome activation. However, GSDMD deficiency did not prevent the MLKL-independent perinatal lethality of gene targeted mice expressing catalytically inactive caspase-8, arguing against a role of pyroptosis (Newton et al., 2019). Therefore, the mechanism by which caspase-8 drives MLKL-independent intestinal pathology in $Fadd^{IEC-KO}$ mice, which depends on GSDMD but not on ASC, is different from the ASC-caspase-1-dependent but GSDMD-independent pathway induced by inhibition of caspase-8 catalytic activity. Yet, RIPK3 contributes to the MLKL-independent functions of caspase-8 both in $Fadd^{IEC-KO}$ mice and in mice expressing catalytically inactive caspase-8 (Fritsch et al., 2019; Newton et al., 2019), although the mechanism by which RIPK3 engages caspase-8 in the absence of FADD remains elusive.

In addition to TNFR1, we identified ZBP1 as a key driver of RIPK3-dependent intestinal inflammation in $Fadd^{IEC-KO}$ mice. Whereas deficiency of either TNFR1 or ZBP1 alone could

inhibit colitis, only combined loss of both pathways could suppress ileitis, suggesting that TNFR1 and ZBP1 exhibit redundant functions in the ileum but synergize to drive severe inflammation in the colon. Differential expression of ZBP1 and TNFR1 in the two tissues could explain the redundant functions in the small intestine as opposed to the synergistic effect in the colon. Because they show higher expression in the small intestine, either TNFR1 or ZBP1 alone could drive RIPK3 activation above a critical threshold causing ileitis, therefore only combined ablation of both suppresses the pathology. In the colon however, TNFR1 and ZBP1 are expressed at lower amounts and need to synergize to drive RIPK3 activation above the threshold required to cause IEC necroptosis and colitis, therefore ablation of one of the two is sufficient to considerably suppress colon inflammation. TRIF also contributed to epithelial cell death and Paneth cell loss, although to a lesser extent compared to the role of TNFR1 and ZBP1.

Taken together, our results revealed that TNFR1 and ZBP1 drive intestinal inflammation by inducing MLKL-dependent necroptosis and caspase-8-GSDMD-mediated pyroptotic-like death of FADD-deficient IECs. This mechanism could be relevant for the pathogenesis of intestinal inflammation during infections with enteropathogenic bacteria that express effectors targeting FADD, such as the arginine glycosyltransferase NleB1 that glycosylates FADD in the death domain inhibiting its function (Pearson et al., 2013; Scott et al., 2017). Furthermore, our results suggest that ZBP1 could be involved in driving intestinal inflammation in human patients with mutations in the *CASP8* gene, who were reported to develop severe forms of very early onset IBD that was refractory to anti-TNF treatment (Lehle et al., 2019). Moreover, our findings that RIPK1 kinase activity drives ZBP1-mediated necroptosis when caspase-8 is inhibited suggest that RIPK1 kinase inhibitors might be effective in these patients. Based on the identified functional redundancy between ZBP1 and TNFR1 in driving intestinal inflammation in our mouse models, it will also be important to explore the potential role of ZBP1 in inflammatory pathologies that are independent or only partially dependent on TNF.

STAR Methods

Resource Availability

Lead Contact

Further information and reasonable requests for resources and reagents should be directed to and will be fulfilled by the Lead Contact, Manolis Pasparakis (pasparakis@uni-koeln.de).

Materials Availability

Fadd^fl/fl, *Mlkl*^-/-, *Zbp1*^-/-, *Ticam1*^fl/fl and *Ripk1*^D138N/D138N mice can be obtained from Manolis Pasparakis, Institute for Genetics, Cologne Excellence Cluster on Cellular Stress Responses in Aging-Associated Diseases (CECAD), University of Cologne, 50931 Cologne, Germany. Email address: pasparakis@uni-koeln.de. *Casp8*^fl/fl mice can be obtained from Stephen M. Hedrick, Division of Biological Sciences, University of California, San Diego, La Jolla, CA 92093, USA. *Tnfr1*^fl/fl mice can be obtained from George Kollias, Biomedical Sciences Research Center "Alexander Fleming," Vari, GR-16672 Greece. *Ripk3*^fl/fl mice can be obtained from Kim Newton, Department of Physiological Chemistry, Genentech, South San Francisco, CA 94080. *Vil1-cre* mice can be obtained from Jackson Laboratories, JAX# 004586. *Asc*^fl/fl mice can be obtained from Amir Yazdi, Department of Dermatology and Allergology, Aachen.

Data availability

The MicroArray data have been deposited in the Gene Expression Omnibus (GEO) database under the accession number GEO: GSE137281 and GSE137280.

Acknowledgments

Author contributions

R.S. performed all experiments and analyzed data. A.T. contributed to the analysis of microarray gene expression data sets. H.J. and L.W. contributed to the cell death assays in Figure 3G and 3H. M.P. coordinated the project and wrote the paper together with R.S.

Declaration of Interests

M.P. received consulting and speaker fees from Genentech, GSK, Boehringer and Sanofi.

References

Adolph, T.E., Tomczak, M.F., Niederreiter, L., Ko, H.J., Bock, J., Martinez-Naves, E., Glickman, J.N., Tschurtschenthaler, M., Hartwig, J., Hosomi, S.*, et al.* (2013). Paneth cells as a site of origin for intestinal inflammation. Nature *503*, 272-276.

Alvarez-Diaz, S., Dillon, C.P., Lalaoui, N., Tanzer, M.C., Rodriguez, D.A., Lin, A., Lebois, M., Hakem, R., Josefsson, E.C., O'Reilly, L.A.*, et al.* (2016). The Pseudokinase MLKL and the Kinase RIPK3 Have Distinct Roles in Autoimmune Disease Caused by Loss of Death-Receptor-Induced Apoptosis. Immunity *45*, 513-526.

Beisner, D.R., Ch'en, I.L., Kolla, R.V., Hoffmann, A., and Hedrick, S.M. (2005). Cutting edge: innate immunity conferred by B cells is regulated by caspase-8. J Immunol *175*, 3469-3473.

Buhner, S., Buning, C., Genschel, J., Kling, K., Herrmann, D., Dignass, A., Kuechler, I., Krueger, S., Schmidt, H.H., and Lochs, H. (2006). Genetic basis for increased intestinal permeability in families with Crohn's disease: role of CARD15 3020insC mutation? Gut *55*, 342-347.

Chinnaiyan, A.M., Tepper, C.G., Seldin, M.F., O'Rourke, K., Kischkel, F.C., Hellbardt, S., Krammer, P.H., Peter, M.E., and Dixit, V.M. (1996). FADD/MORT1 is a common mediator of CD95 (Fas/APO-1) and tumor necrosis factor receptor-induced apoptosis. J Biol Chem *271*, 4961-4965.

Dannappel, M., Vlantis, K., Kumari, S., Polykratis, A., Kim, C., Wachsmuth, L., Eftychi, C., Lin, J., Corona, T., Hermance, N.*, et al.* (2014). RIPK1 maintains epithelial homeostasis by inhibiting apoptosis and necroptosis. Nature *513*, 90-94.

Drexler, S.K., Bonsignore, L., Masin, M., Tardivel, A., Jackstadt, R., Hermeking, H., Schneider, P., Gross, O., Tschopp, J., and Yazdi, A.S. (2012). Tissue-specific opposing functions of the inflammasome adaptor ASC in the regulation of epithelial skin carcinogenesis. Proc Natl Acad Sci U S A *109*, 18384-18389.

Eftychi, C., Schwarzer, R., Vlantis, K., Wachsmuth, L., Basic, M., Wagle, P., Neurath, M.F., Becker, C., Bleich, A., and Pasparakis, M. (2019). Temporally Distinct Functions of the Cytokines IL-12 and IL-23 Drive Chronic Colon Inflammation in Response to Intestinal Barrier Impairment. Immunity *51*, 367-380 e364.

Fritsch, M., Gunther, S.D., Schwarzer, R., Albert, M.C., Schorn, F., Werthenbach, J.P., Schiffmann, L.M., Stair, N., Stocks, H., Seeger, J.M., *et al.* (2019). Caspase-8 is the molecular switch for apoptosis, necroptosis and pyroptosis. Nature *575*, 683-687.

Gunther, C., Martini, E., Wittkopf, N., Amann, K., Weigmann, B., Neumann, H., Waldner, M.J., Hedrick, S.M., Tenzer, S., Neurath, M.F., and Becker, C. (2011). Caspase-8 regulates TNF-alpha-induced epithelial necroptosis and terminal ileitis. Nature *477*, 335-339.

Jiao, H., Wachsmuth, L., Kumari, S., Schwarzer, R., Lin, J., Eren, R.O., Fisher, A., Lane, R., Young, G.R., Kassiotis, G., *et al.* (2020). Z-nucleic-acid sensing triggers ZBP1-dependent necroptosis and inflammation. Nature *580*, 391-395.

Kaiser, W.J., Upton, J.W., Long, A.B., Livingston-Rosanoff, D., Daley-Bauer, L.P., Hakem, R., Caspary, T., and Mocarski, E.S. (2011). RIP3 mediates the embryonic lethality of caspase-8-deficient mice. Nature *471*, 368-372.

Katz, K.D., Hollander, D., Vadheim, C.M., McElree, C., Delahunty, T., Dadufalza, V.D., Krugliak, P., and Rotter, J.I. (1989). Intestinal permeability in patients with Crohn's disease and their healthy relatives. Gastroenterology *97*, 927-931.

Kiesslich, R., Duckworth, C.A., Moussata, D., Gloeckner, A., Lim, L.G., Goetz, M., Pritchard, D.M., Galle, P.R., Neurath, M.F., and Watson, A.J. (2012). Local barrier dysfunction identified by confocal laser endomicroscopy predicts relapse in inflammatory bowel disease. Gut *61*, 1146-1153.

Kuriakose, T., Man, S.M., Malireddi, R.K., Karki, R., Kesavardhana, S., Place, D.E., Neale, G., Vogel, P., and Kanneganti, T.D. (2016). ZBP1/DAI is an innate sensor of influenza virus triggering the NLRP3 inflammasome and programmed cell death pathways. Sci Immunol *1*.

Lawlor, K.E., Khan, N., Mildenhall, A., Gerlic, M., Croker, B.A., D'Cruz, A.A., Hall, C., Kaur Spall, S., Anderton, H., Masters, S.L., *et al.* (2015). RIPK3 promotes cell death and NLRP3 inflammasome activation in the absence of MLKL. Nat Commun *6*, 6282.

Lee, B.L., Mirrashidi, K.M., Stowe, I.B., Kummerfeld, S.K., Watanabe, C., Haley, B., Cuellar, T.L., Reichelt, M., and Kayagaki, N. (2018). ASC- and caspase-8-dependent apoptotic pathway diverges from the NLRC4 inflammasome in macrophages. Sci Rep *8*, 3788.

Lehle, A.S., Farin, H.F., Marquardt, B., Michels, B.E., Magg, T., Li, Y., Liu, Y., Ghalandary, M., Lammens, K., Hollizeck, S., *et al.* (2019). Intestinal Inflammation and Dysregulated Immunity in Patients With Inherited Caspase-8 Deficiency. Gastroenterology *156*, 275-278.

Lin, J., Kumari, S., Kim, C., Van, T.M., Wachsmuth, L., Polykratis, A., and Pasparakis, M. (2016). RIPK1 counteracts ZBP1-mediated necroptosis to inhibit inflammation. Nature *540*, 124-128.

Madison, B.B., Dunbar, L., Qiao, X.T., Braunstein, K., Braunstein, E., and Gumucio, D.L. (2002). Cis elements of the villin gene control expression in restricted domains of the vertical (crypt) and horizontal (duodenum, cecum) axes of the intestine. J Biol Chem *277*, 33275-33283.

Man, S.M., Tourlomousis, P., Hopkins, L., Monie, T.P., Fitzgerald, K.A., and Bryant, C.E. (2013). Salmonella infection induces recruitment of Caspase-8 to the inflammasome to modulate IL-1beta production. J Immunol *191*, 5239-5246.

Mascarenhas, D.P.A., Cerqueira, D.M., Pereira, M.S.F., Castanheira, F.V.S., Fernandes, T.D., Manin, G.Z., Cunha, L.D., and Zamboni, D.S. (2017). Inhibition of caspase-1 or gasdermin-D enable caspase-8 activation in the Naip5/NLRC4/ASC inflammasome. PLoS Pathog *13*, e1006502.

Masumoto, J., Dowds, T.A., Schaner, P., Chen, F.F., Ogura, Y., Li, M., Zhu, L., Katsuyama, T., Sagara, J., Taniguchi, S., *et al.* (2003). ASC is an activating adaptor for NF-kappa B and caspase-8-dependent apoptosis. Biochem Biophys Res Commun *303*, 69-73.

Mc Guire, C., Volckaert, T., Wolke, U., Sze, M., de Rycke, R., Waisman, A., Prinz, M., Beyaert, R., Pasparakis, M., and van Loo, G. (2010). Oligodendrocyte-specific FADD deletion protects mice from autoimmune-mediated demyelination. J Immunol *185*, 7646-7653.

Moriwaki, K., Balaji, S., Bertin, J., Gough, P.J., and Chan, F.K. (2017). Distinct Kinase-Independent Role of RIPK3 in CD11c(+) Mononuclear Phagocytes in Cytokine-Induced Tissue Repair. Cell Rep *18*, 2441-2451.

Moriwaki, K., Balaji, S., McQuade, T., Malhotra, N., Kang, J., and Chan, F.K. (2014). The necroptosis adaptor RIPK3 promotes injury-induced cytokine expression and tissue repair. Immunity *41*, 567-578.

Muzio, M., Chinnaiyan, A.M., Kischkel, F.C., O'Rourke, K., Shevchenko, A., Ni, J., Scaffidi, C., Bretz, J.D., Zhang, M., Gentz, R.*, et al.* (1996). FLICE, a novel FADD-homologous ICE/CED-3-like protease, is recruited to the CD95 (Fas/APO-1) death--inducing signaling complex. Cell *85*, 817-827.

Nenci, A., Becker, C., Wullaert, A., Gareus, R., van Loo, G., Danese, S., Huth, M., Nikolaev, A., Neufert, C., Madison, B.*, et al.* (2007). Epithelial NEMO links innate immunity to chronic intestinal inflammation. Nature *446*, 557-561.

Newton, K., Dugger, D.L., Maltzman, A., Greve, J.M., Hedehus, M., Martin-McNulty, B., Carano, R.A., Cao, T.C., van Bruggen, N., Bernstein, L.*, et al.* (2016a). RIPK3 deficiency or catalytically inactive RIPK1 provides greater benefit than MLKL deficiency in mouse models of inflammation and tissue injury. Cell Death Differ *23*, 1565-1576.

Newton, K., Wickliffe, K.E., Maltzman, A., Dugger, D.L., Reja, R., Zhang, Y., Roose-Girma, M., Modrusan, Z., Sagolla, M.S., Webster, J.D., and Dixit, V.M. (2019). Activity of caspase-8 determines plasticity between cell death pathways. Nature *575*, 679-682.

Newton, K., Wickliffe, K.E., Maltzman, A., Dugger, D.L., Strasser, A., Pham, V.C., Lill, J.R., Roose-Girma, M., Warming, S., Solon, M.*, et al.* (2016b). RIPK1 inhibits ZBP1-driven necroptosis during development. Nature *540*, 129-133.

Nogusa, S., Thapa, R.J., Dillon, C.P., Liedmann, S., Oguin, T.H., 3rd, Ingram, J.P., Rodriguez, D.A., Kosoff, R., Sharma, S., Sturm, O.*, et al.* (2016). RIPK3 Activates Parallel Pathways of MLKL-Driven Necroptosis and FADD-Mediated Apoptosis to Protect against Influenza A Virus. Cell Host Microbe *20*, 13-24.

Nolte, H., MacVicar, T.D., Tellkamp, F., and Kruger, M. (2018). Instant Clue: A Software Suite for Interactive Data Visualization and Analysis. Sci Rep *8*, 12648.

Oberst, A., Dillon, C.P., Weinlich, R., McCormick, L.L., Fitzgerald, P., Pop, C., Hakem, R., Salvesen, G.S., and Green, D.R. (2011). Catalytic activity of the caspase-8-FLIP(L) complex inhibits RIPK3-dependent necrosis. Nature *471*, 363-367.

Orning, P., Weng, D., Starheim, K., Ratner, D., Best, Z., Lee, B., Brooks, A., Xia, S., Wu, H., Kelliher, M.A.*, et al.* (2018). Pathogen blockade of TAK1 triggers caspase-8-dependent cleavage of gasdermin D and cell death. Science *362*, 1064-1069.

Pasparakis, M., and Vandenabeele, P. (2015). Necroptosis and its role in inflammation. Nature *517*, 311-320.

Pearson, J.S., Giogha, C., Ong, S.Y., Kennedy, C.L., Kelly, M., Robinson, K.S., Lung, T.W., Mansell, A., Riedmaier, P., Oates, C.V.*, et al.* (2013). A type III effector antagonizes death receptor signalling during bacterial gut infection. Nature *501*, 247-251.

Pierini, R., Juruj, C., Perret, M., Jones, C.L., Mangeot, P., Weiss, D.S., and Henry, T. (2012). AIM2/ASC triggers caspase-8-dependent apoptosis in Francisella-infected caspase-1-deficient macrophages. Cell Death Differ *19*, 1709-1721.

Polykratis, A., Hermance, N., Zelic, M., Roderick, J., Kim, C., Van, T.M., Lee, T.H., Chan, F.K.M., Pasparakis, M., and Kelliher, M.A. (2014). Cutting edge: RIPK1 Kinase inactive mice are viable and protected from TNF-induced necroptosis in vivo. J Immunol *193*, 1539-1543.

Rauch, I., Deets, K.A., Ji, D.X., von Moltke, J., Tenthorey, J.L., Lee, A.Y., Philip, N.H., Ayres, J.S., Brodsky, I.E., Gronert, K., and Vance, R.E. (2017). NAIP-NLRC4 Inflammasomes Coordinate Intestinal Epithelial Cell Expulsion with Eicosanoid and IL-18 Release via Activation of Caspase-1 and -8. Immunity *46*, 649-659.

Sagulenko, V., Thygesen, S.J., Sester, D.P., Idris, A., Cridland, J.A., Vajjhala, P.R., Roberts, T.L., Schroder, K., Vince, J.E., Hill, J.M.*, et al.* (2013). AIM2 and NLRP3 inflammasomes activate both apoptotic and pyroptotic death pathways via ASC. Cell Death Differ *20*, 1149-1160.

Sarhan, J., Liu, B.C., Muendlein, H.I., Li, P., Nilson, R., Tang, A.Y., Rongvaux, A., Bunnell, S.C., Shao, F., Green, D.R., and Poltorak, A. (2018). Caspase-8 induces cleavage of gasdermin D to elicit pyroptosis during Yersinia infection. Proc Natl Acad Sci U S A *115*, E10888-E10897.

Scott, N.E., Giogha, C., Pollock, G.L., Kennedy, C.L., Webb, A.I., Williamson, N.A., Pearson, J.S., and Hartland, E.L. (2017). The bacterial arginine glycosyltransferase effector NleB preferentially modifies Fas-associated death domain protein (FADD). J Biol Chem *292*, 17337-17350.

Stolzer, I., Kaden-Volynets, V., Ruder, B., Letizia, M., Bittel, M., Rausch, P., Basic, M., Bleich, A., Baines, J.F., Neurath, M.F.*, et al.* (2020). Environmental Microbial Factors Determine the Pattern of Inflammatory Lesions in a Murine Model of Crohn's Disease-Like Inflammation. Inflamm Bowel Dis *26*, 66-79.

Takahashi, N., Vereecke, L., Bertrand, M.J., Duprez, L., Berger, S.B., Divert, T., Goncalves, A., Sze, M., Gilbert, B., Kourula, S.*, et al.* (2014). RIPK1 ensures intestinal homeostasis by protecting the epithelium against apoptosis. Nature *513*, 95-99.

Turner, J.R. (2009). Intestinal mucosal barrier function in health and disease. Nat Rev Immunol *9*, 799-809.

Upton, J.W., Kaiser, W.J., and Mocarski, E.S. (2012). DAI/ZBP1/DLM-1 complexes with RIP3 to mediate virus-induced programmed necrosis that is targeted by murine cytomegalovirus vIRA. Cell Host Microbe *11*, 290-297.

Van Hauwermeiren, F., Armaka, M., Karagianni, N., Kranidioti, K., Vandenbroucke, R.E., Loges, S., Van Roy, M., Staelens, J., Puimege, L., Palagani, A.*, et al.* (2013). Safe TNF-based antitumor therapy following p55TNFR reduction in intestinal epithelium. J Clin Invest *123*, 2590-2603.

Vlantis, K., Wullaert, A., Polykratis, A., Kondylis, V., Dannappel, M., Schwarzer, R., Welz, P., Corona, T., Walczak, H., Weih, F.*, et al.* (2016). NEMO Prevents RIP Kinase 1-Mediated Epithelial Cell Death and Chronic Intestinal Inflammation by NF-kappaB-Dependent and -Independent Functions. Immunity *44*, 553-567.

Weinlich, R., Oberst, A., Dillon, C.P., Janke, L.J., Milasta, S., Lukens, J.R., Rodriguez, D.A., Gurung, P., Savage, C., Kanneganti, T.D., and Green, D.R. (2013). Protective roles for caspase-8 and cFLIP in adult homeostasis. Cell Rep *5*, 340-348.

Welz, P.S., Wullaert, A., Vlantis, K., Kondylis, V., Fernandez-Majada, V., Ermolaeva, M., Kirsch, P., Sterner-Kock, A., van Loo, G., and Pasparakis, M. (2011). FADD prevents RIP3-mediated epithelial cell necrosis and chronic intestinal inflammation. Nature *477*, 330-334.

Wittkopf, N., Gunther, C., Martini, E., He, G., Amann, K., He, Y.W., Schuchmann, M., Neurath, M.F., and Becker, C. (2013). Cellular FLICE-like inhibitory protein secures intestinal epithelial cell survival and immune homeostasis by regulating caspase-8. Gastroenterology *145*, 1369-1379.

Zhang, H., Zhou, X., McQuade, T., Li, J., Chan, F.K., and Zhang, J. (2011). Functional complementation between FADD and RIP1 in embryos and lymphocytes. Nature *471*, 373-376.

STAR Methods

Key Resources Table

REAGENT or RESOURCE	SOURCE	IDENTIFIER
Antibodies		
CD45	BD Biosciences	Cat# 560510, RRID:AB_1645208
cleaved-Caspase-3	Cell Signaling	Cat# 9661, RRID:AB_2341188
Lysozyme	Dako	Cat# F0372
cleaved-Caspase-8	Cell Signaling	Cat# 8592, RRID:AB_10891784
Anti-rabbit alexa 488	ThermoScientific	Cat# A-11008, RRID:AB_143165
Anti-rabbit-IgG, HRP conjugated	GE Healthcare	Cat# NA934, RRID:AB_772206
Anti-mouse-IgG, HRP conjugated	GE Healthcare	Cat# NA931, RRID:AB_772210
Anti-rat-IgG, HRP conjugated	Jackson Laboratories	Cat# 112-035-003, RRID:AB_2338128
Anti-goat-IgG, HRP conjugated	Jackson Laboratories	Cat# 705-035-003, RRID:AB_2340390
mFADD	Millipore	Cat# 05-486, RRID:AB_2100627
mMLKL	Millipore	Cat#MABC604
mRIPK1	BD Biosciences	Cat# 610459, RRID:AB_397832
mRIPK3	Enzo LifeSciences	Cat# ADI-905-242-100, RRID:AB_2039527
mGAPDH	Novus Biologicals	Cat# NB300-221, RRID:AB_10077627
mGSDMD	Abcam	Cat# 219800
CRE	Novagen	Cat# 69050-3, RRID:AB_2314229
mCaspase-8 (total)	Alexis	Cat# ALX-804-447, RRID:AB_2243830
mZBP1	Adipogen	Cat# AG-20B-0010, RRID:AB_2490191
mACTIN	SantaCruz	Cat# sc-1616, RRID:AB_630836
Alpha-Tubulin	Sigma	Cat# T6074, RRID:AB_477582
mASC (Immunoblot)	Adipogen	Cat# AG-25B-0006, RRID:AB_2490440
mASC (Immunohistochemistry)	Santa Cruz	Cat#sc-22514-R, RRID:AB_217874
Phosphorylated RIPK1 (S166)	Cell Signaling	Cat# 31122, RRID:AB_2799000
Phosphorylated MLKL (S345)	Cell Signaling	Cat# 37333, RRID:AB_2799112
Chemicals		
Doxycycline	Sigma Aldrich	Cat#D9891
Necrostatin 1s	BioCat	Cat#2263-5-BV
Puromycin	Sigma Aldrich	Cat#P8833-25MG
Polybrene	Sigma Aldrich	Cat#H9268
YOYO™-1 Iodide (491/509)	ThermoScientific	Cat#Y3601
Emricasan	Selleckchem	Cat#S7775
Recombinant mouse interferon gamma	ImmunoTools	Cat#12343537
Plasmids		
pMD2.G	Addgene	Cat#12259

psPAX2	Addgene	Cat#12260
pCW-sFLAG-ZBP1	this paper	N/A
Critical Commercial Assays		
X-tremeGENE HD DNA Transfection Reagent	Roche	Cat#06366236001
NucleoSpin RNA isolation kit	Macherey Nagel	Cat#740955.250
SuperScript III Reverse Transcriptase	ThermoScientific	Cat# 18080044
Clariom-S-Assay	ThermoScientific	Cat#902930
Deposited Data		
RNA MicroArray Data Colon	This paper	https://www.ncbi.nlm.nih.gov/geo/query/acc.cgi?acc=GSE137281
RNA MicroArray Data Ileum	This paper	https://www.ncbi.nlm.nih.gov/geo/query/acc.cgi?acc=GSE137280
Experimental Models: Organisms/Strains		
Mouse: $Fadd^{fl/fl}$, C57BL/6N	(Mc Guire et al., 2010)	N/A
Mouse: $Mlkl^{-/-}$, C57BL/6N	(Dannappel et al., 2014)	N/A
Mouse: $Casp8^{fl/fl}$, C57BL/6N	(Gunther et al., 2011)	N/A
Mouse: $Tnfr1^{fl/fl}$, C57BL/6N	(Van Hauwermeiren et al., 2013)	N/A
Mouse: $Asc^{fl/fl}$, C57BL/6N	(Drexler et al., 2012)	N/A
Mouse: $Ripk3^{fl/fl}$, C57BL/6N	(Newton et al., 2016)	N/A
Mouse: $Zbp1^{-/-}$, C57BL/6N	(Jiao et al., 2020)	
Mouse: $Ticam1^{fl/fl}$, C57BL/6N	(Dannappel et al., 2014)	N/A
Mouse: $Ripk1^{D138N/D138N}$, C57BL/6N	(Polykratis et al., 2014)	N/A
Mouse: $Vil1$-Cre: B6.Cg-Tg(Vil1-cre)997Gum/J	The Jackson Laboratory	JAX# 004586
Mouse: $Gsdmd^{-/-}$, C57BL/6N	This paper	N/A
Oligonucleotides		
murine $Gsdmd$ sgRNA1: 5'-GCAGTATACACACATTCATGG-3'	this paper	N/A
murine $Gsdmd$ sgRNA2: 5'-GCGTGTGACTCAGAAGACCT-3'	this paper	N/A
TagMan Probes		
Ccl2	ThermoScientific	Mm00441242_m1
Il1b	ThermoScientific	Mm00434228_m1
Il6	ThermoScientific	Mm00446190_m1
Lyz1	ThermoScientific	Mm00657323_m1
Defa-rs1	ThermoScientific	Mm00655851_gH
Ang4	ThermoScientific	Mm03647554_g1
Tbp	ThermoScientific	Mm00446973_m1
Software and Algorithms	ThermoScientific	
Prism 6.0	Graphpad Inc	RRID: SCR_002798
Instant Clue	(Nolte et al., 2018)	http://www.instantclue.uni-koeln.de/

References for STAR Methods Key Resources

Dannappel, M., Vlantis, K., Kumari, S., Polykratis, A., Kim, C., Wachsmuth, L., Eftychi, C., Lin, J., Corona, T., Hermance, N.*, et al.* (2014). RIPK1 maintains epithelial homeostasis by inhibiting apoptosis and necroptosis. Nature *513*, 90-94.

Gunther, C., Martini, E., Wittkopf, N., Amann, K., Weigmann, B., Neumann, H., Waldner, M.J., Hedrick, S.M., Tenzer, S., Neurath, M.F., and Becker, C. (2011). Caspase-8 regulates TNF-alpha-induced epithelial necroptosis and terminal ileitis. Nature *477*, 335-339.

Jiao, H., Wachsmuth, L., Kumari, S., Schwarzer, R., Lin, J., Eren, R.O., Fisher, A., Lane, R., Young, G.R., Kassiotis, G.*, et al.* (2020). Z-nucleic-acid sensing triggers ZBP1-dependent necroptosis and inflammation. Nature *580*, 391-395

Mc Guire, C., Volckaert, T., Wolke, U., Sze, M., de Rycke, R., Waisman, A., Prinz, M., Beyaert, R., Pasparakis, M., and van Loo, G. (2010). Oligodendrocyte-specific FADD deletion protects mice from autoimmune-mediated demyelination. J Immunol *185*, 7646-7653.

Newton, K., Dugger, D.L., Maltzman, A., Greve, J.M., Hedehus, M., Martin-McNulty, B., Carano, R.A., Cao, T.C., van Bruggen, N., Bernstein, L.*, et al.* (2016). RIPK3 deficiency or catalytically inactive RIPK1 provides greater benefit than MLKL deficiency in mouse models of inflammation and tissue injury. Cell Death Differ *23*, 1565-1576.

Nolte, H., MacVicar, T.D., Tellkamp, F., and Kruger, M. (2018). Instant Clue: A Software Suite for Interactive Data Visualization and Analysis. Sci Rep *8*, 12648.

Polykratis, A., Hermance, N., Zelic, M., Roderick, J., Kim, C., Van, T.M., Lee, T.H., Chan, F.K.M., Pasparakis, M., and Kelliher, M.A. (2014). Cutting edge: RIPK1 Kinase inactive mice are viable and protected from TNF-induced necroptosis in vivo. J Immunol *193*, 1539-1543.

Van Hauwermeiren, F., Armaka, M., Karagianni, N., Kranidioti, K., Vandenbroucke, R.E., Loges, S., Van Roy, M., Staelens, J., Puimege, L., Palagani, A.*, et al.* (2013). Safe TNF-based antitumor therapy following p55TNFR reduction in intestinal epithelium. J Clin Invest *123*, 2590-2603.

Experimental model and subject details

Mice

Fadd$^{fl/fl}$ (Mc Guire et al., 2010), *Mlkl*$^{-/-}$, *Ticam1*$^{fl/fl}$ (Dannappel et al., 2014), *Casp8*$^{fl/fl}$ (Beisner et al., 2005), *Ripk1*$^{D138N/D138N}$ mice (Polykratis et al., 2014), *Vil1-cre* (Madison et al., 2002), *Tnfr1*$^{fl/fl}$ (Van Hauwermeiren et al., 2013), *Asc*$^{fl/fl}$ (Drexler et al., 2012) and *Ripk3*$^{fl/fl}$ (Newton et al., 2016a) were described previously. *Zbp1*$^{-/-}$ mice were generated using CrispR/Cas9 mediated gene disruption in fertilized oocytes (Jiao et al., 2020). *Gsdmd*$^{-/-}$ mice were generated in this study. Mice of the indicated genotype were assigned at random to groups. Mouse studies were performed in a blinded fashion. All mice were maintained in C57BL/6N background. Mice in other than C57BL/6N genetic background were first backcrossed for at least ten generations onto the C57BL/6N background except for *Fadd*$^{IEC-KO}$ *Mlkl*$^{-/-}$ *Gsdmd*$^{-/-}$ mice as described in Figure 7. Mice were maintained at the SPF animal facilities of the CECAD Research Center, University of Cologne, under a 12 hour light cycle and given water ad libitum and a regular chow diet (Harlan, diet no. 2918). All animal procedures were conducted in accordance with European, national, and institutional guidelines, and protocols were approved by local government authorities (Landesamt für Natur, Umwelt und Verbraucherschutz Nordrhein-Westfalen). Animals requiring medical attention were provided with appropriate care. No other exclusion criteria existed.

Targeting of *Gsdmd* in mouse zygotes
Gsdmd$^{-/-}$ mice were generated using CrispR/Cas9 technology as previously described (Eftychi et al., 2019). Fertilized oocytes obtained from breedings of *Fadd*$^{fl/fl}$ *Mlkl*$^{-/-}$ *Vil1-cre*$^{tg/wt}$ male mice with *Fadd*$^{fl/fl}$ *Mlkl*$^{-/wt}$ or *Fadd*$^{fl/fl}$ *Mlkl*$^{-/-}$ female mice were microinjected with two short guide (sg)RNAs targeting the *Gsdmd* gene (5'- GCAGTATACACACATTCA-3' and 5'-GCGTGTGACTCAGAAGACCT-3') together with Cas9 mRNA (TriLink). Mice obtained in the F0 generation were sequenced for *Gsdmd* allele mutations and mice with targeted inactivation of *Gsdmd* were intercrossed to generate *Fadd*$^{IEC-KO}$ *Mlkl*$^{-/-}$ *Gsdmd*$^{-/-}$ mice in the F1 generation. F1 mice were screened for GSDMD and MLKL deficiency using immunoblot analysis of spleen lysates.

Method details

Cell culture
Cell lines were maintained at 37°C and 5% CO_2. All cell lines were cultured in 10%FCS, 1% P/S, 1% L-Glutamate, 1mM Sodium Pyruvate (ThermoFisher Scientific, #11360) and DMEM-Dulbecco's Modified Eagle Medium (ThermoFisher, #41965-039).

Lentiviral production
HEK293 cells were transfected with pCW-sFLAG-mZBP1 (10μg), psPAX2 (5μg) (Addgene, #12260) and pMD2.G (5μg) (Addgene, #12259) plasmid to produce lentivirus pCW-sFLAG-mZBP1. In detail, plasmids were mixed with 500μl 0.25M $CaCl_2$. Then, 500μl 2xHBS was added slowly while stirring the solution using pipette tip. After 5 min of incubation (RT), the $CaCl_2$-HBS-plasmid solution was added dropwise to HEK293 cells cultured in 10ml culture medium. HEK293 cells were fed with fresh medium 1h prior to transfection. After 24h (day1), medium was replaced with fresh culture medium. Supernatant containing viruses were collected on day 2 and 3.

Generation of immortalized mouse embryonic fibroblasts with doxycycline-inducible ZBP1 expression
Immortalized mouse embryonic fibroblasts (iMEFs) overexpressing mouse ZBP1 (ENSMUST00000029018.13) were generated using lentiviral gene transfer. 48h prior to transduction, 200.000 cells/well were seeded in a 6-well plate (Sigma Aldrich, # CLS3335). Cells were incubated with 1.5ml fresh medium + 750μl Virus-Supernatant + 8μg/ml Polybrene (Sigma Aldrich, #H9268) for 24h. On the next day, virus containing medium was removed and

replaced with fresh medium containing 2μg/ml puromycin. After 48h, puromycin was removed and cell pools were used for experiments.

Cell death assay

iMEFs were seeded 24h prior to stimulation in a 96 well plate (Sigma-Aldrich, CLS3340-50EA) (1×10^4 cells per well). On the day of experiment, for ZBP1 induced expression cells were pre-stimulated with Doxycycline (Sigma Aldrich D9891) for a minimum of 4 hours. Then, 5μM Emricasan (Selleckchem, #S7775), 20μM Necrostatin 1s (BioCat, 2263-5-BV) or a combination was added. For primary lung fibroblasts, cells were seeded 24h prior to recombinant mouse interferon gamma treatment (1000U/ml, ImmunoTools, #12343537). After 24h (48h after seeding), cells were stimulated with Emricasan. Cell death assays were performed using the IncuCyte bioimaging platform (Essen); four images per well were captured, analyzed and averaged. Cell death was measured by YOYO™-1 Iodide (491/509) incorporation (ThermoScientific, Cat#Y3601).

RNA isolation from tissues

Isolation of RNA from colon and small intestine tissue was performed using a NucleoSpin RNA isolation kit (Macherey Nagel Ref. 740955.250). Most procedures were done according to manufacturer's instructions. However, rDNAse treatment was increased to 45 minutes at RT. Furthermore, tissue lysis in buffer RA1 was performed at 4°C. RNA was eluted in 60μl RNAse-free H2O.

MicroArray analysis

RNA quality was evaluated based on RNA integrity number (RIN) and OD260/280 and OD260/230 ratios. RIN value was determined using TapeStation4200 and RNA ScreenTapes (Agilent Technologies). Labelled cDNA was generated using GeneChip WT PLUS Reagent Kit (Affymetrix). Gene expression was determined using Clariome-S-Assay, mouse (ThermoFisher, 902930, Format 169). Sample exclusion criteria were OD260/280<1.8, OD260/230<1.5 and RIN<7. Three samples with a RIN below 7 (Small intestine tissue samples, *Fadd*^IEC-KO *Zbp1*^-/-, RIN values: 6.9, 6.3, 6) were included for the analysis. Gene expression data were visualized using InstantClue (Nolte et al., 2018).

For MicroArray analysis of colon samples of *Fadd*^IEC-KO and *Casp8*^IEC-KO mice, 10 samples were used due to stronger variation of the colitis phenotype. Otherwise, 5 mice were used per group as indicated. For colon data sets, visualizing average gene expression ($\log_2$) using HeatmapCluster-analysis was done by including significantly upregulated genes (cut-off: fold change ≥ ±1.5, p-value <0.05) in *Fadd*^IEC-KO (920 genes) or *Casp8*^IEC-KO (140 genes) compared to their respective floxed controls. If graphs contain both *Fadd*^IEC-KO and *Casp8*^IEC-KO mice, graphs were created using 920 genes upregulated in *Fadd*^IEC-KO mice and 44 genes specifically upregulated in *Casp8*^IEC-KO mice (96 significantly (cut-off: fold change ≥ ±1.5, p-value <0.05) upregulated genes were found in both genotypes and only included once).

For ileum data sets, visualizing average gene expression ($\log_2$) using HeatmapCluster-analysis was done by including significantly upregulated genes (cut-off: fold change ≥ ±1.5, p-value <0.05) in *Fadd*^IEC-KO (370 genes) or *Casp8*^IEC-KO (250 genes) compared to their respective floxed controls. If graphs contain both *Fadd*^IEC-KO and *Casp8*^IEC-KO mice, graphs were created using 370 genes upregulated in *Fadd*^IEC-KO mice and 128 genes specifically upregulated in *Casp8*^IEC-KO mice (122 significantly (cut-off: fold change ≥ ±1.5, p-value <0.05) upregulated genes were found in both genotypes and only included once).

For the identification of genes for which the expression correlated with colitis severity in *Fadd*^IEC-KO and *Casp8*^IEC-KO mice, principal component analysis including all genes was performed. Then, principal component 1 was correlated to colitis severity (histology scores) and the top25 up or downregulated genes selected and visualized using heatmap clustering.

Quantitative RT-PCR

cDNA was prepared using Superscript III cDNA-synthesis kit (ThermoScientific, 18080-044), qRT-PCR was performed with TaqMan probes (Life Technologies) with TATA-box-binding protein (Tbp) serving as reference genes. Data were analyzed according to the CT method and are represented in dot plot graphs as fold change relative to CRE-negative littermates. Taqman probes used: *Ccl2* (ThermoScientific, Mm00441242_m1), *Il1b* (ThermoScientific, Mm00434228_m1), *Il6* (ThermoScientific, Mm00446190_m1), *Lyz1* (ThermoScientific, Mm00657323_m1), *Defa-rs2* (ThermoScientific, Mm00655851_gH), *Ang4* (ThermoScientific, Mm03647554_g1), Tbp (ThermoScientific, Mm00446973_m1).

Tissue preparation

Mice were sacrificed using cervical dislocation. The colon and small intestine were prepared and washed with PBS. A ~0,5cm piece of the colon located ~1-1.5cm prior to the anus and a ~0,5cm piece of the small intestinal located ~1-1.5cm prior to the caecum were snap frozen on dry ice for RNA expression analysis and stored at -80°C until further processing. The remaining colon tissue and ~8-9cm of the most distal small intestine (designated ileum) tissue were cut longitudinally and washed in PBS to remove feces. Intestinal tissues were rolled up from proximal to distal and fixed in 4% PFA O/N at 4°C.

Histopathological analysis

Histopathological evaluation was performed on 3 µm thick H&E-stained sections of paraffin-embedded swiss-rolls of intestinal tissues, using a modified version of a the scoring system described in (Adolph et al., 2013). In brief, histopathology scores are composed of four parameters: epithelial hyperplasia, quantity and localization of tissue inflammation, epithelial cell death and epithelial injury. An "area factor" for the fraction of affected tissue was assigned and multiplied with the respective parameter score. (1=0-25%; 2=25-50%; 3=50-75%, 4=75-100%). If different severities for the same parameter were observed in the same sample, each area was judged individually and multiplied with the correlating area factor. Area factors for a given sample always added up to 4. The histology score was calculated as the sum of all parameter scores multiplied with their area factors. Maximum score was 64. Scores and ulcer quantification are based on one swiss-roll section per mouse and were performed in a blinded fashion.

Histological sub-scores:
1. crypt hyperplasia
   0 = normal crypt proliferation
   1 = signs of increased proliferating – expansion of TA compartment
   2 = obvious increase in proliferating cells – reduced numbers of differentiated cells; increased nuclear/cytoplasm ratio; differentiated cells mainly in the upper part of the crypt; shortening of villi
   3 = almost complete absence of differentiated cells, severe villus atrophy (small intestine)
2. epithelial injury/erosion
   0 = no alterations in epithelial structure, no mucosal damage
   1 = discrete focal lympho-epithelial erosions
   2 = surface mucosal erosion
   3 = extensive epithelial erosions (ulcers, mucosa denudation and damage extending into deeper layers of the bowel wall
3. extend of inflammation in the tissue
   0 = absent
   1 = increased amounts of immune cells in the lamina propria
   2 = inflammation extending into the submucosa
   3 = transmural inflammation extending into muscularis and serosa
4. death of epithelial cells
   0 = absent (except for physiologically standard cell death)
   1 = increase in the occurrence of individual dying IECs or small clusters of dying cells

2 = clearly visible IEC death with cell shedding, areas with epithelial thinning and early stages of crypt abscess formation
3 = clear presence of erosive lesions (ulcer formation)

Control groups of mice

In all experiments, "control" groups of mice included healthy littermates with homozygous or heterozygous loxP-flanked *Fadd* or *Casp8* alleles that do not express *Vil1*-Cre (*Fadd*$^{fl/fl}$ or *Fadd*$^{fl/WT}$, *Casp8*$^{fl/fl}$ or *Casp8*$^{fl/WT}$), or with heterozygous loxP-flanked *Fadd* or *Casp8* alleles that also express *Vil1*-cre (*Fadd*$^{fl/WT}$ x *Vil1*-cre, *Casp8*$^{fl/WT}$ x *Vil1*-cre), which also carried loxP flanked or knockout alleles of the additional genes employed for the rescue of the intestinal pathology in *Fadd*$^{IEC-KO}$ and *Casp8*$^{IEC-KO}$ mice. A detailed list of all the mice analyzed within this study is included in Table S2.

Quantification of crypts containing cleaved caspase-8$^+$ cells

Quantification of cleaved caspase-8 positive cells was performed on histological sections immunostained with antibodies against cleaved Caspase-8. 100 crypts were analyzed per mouse. Positive crypts contained a minimum of 1 stained cell. Each mouse was counted twice and the average was used. Counting was performed in a blinded fashion.

Hematoxylin & Eosin staining of paraffin-fixed tissues

Paraffin-embedded 3 μm-thick tissue sections were de-paraffinized with xylene and re-hydrated with ethanol/water solutions (100% Ethanol, 96% Ethanol, 75% Ethanol, 0% Ethanol). Sections were stained for 2 minutes in hematoxylin, differentiated in tap water (15 min) and incubated for 1 minute in eosin. Stained sections were de-hydrated using ethanol/water solutions and fixed in xylene. Slides were mounted with Entellan.

Immunohistochemistry

Paraffin sections were rehydrated using xylene and decreasing amounts of ethanol. Epitope retrieval was achieved using Proteinase K digest (for CD45 and Lysozyme) or heat-induced epitope retrieval in citrate, TRIS buffer, pH 6 (for cleaved Caspase-3). Endogenous peroxidase was blocked in Peroxidase blocking buffer for 15min at RT. Endogenous avidin was blocked using biotin from (1:100 dilution) from Avidin/Biotin blocking kit (Vector, no. SP-2001). Sections were incubated at 4°C O/N with primary antibodies and avidin (1:100 dilution) from Avidin/Biotin blocking kit (Vector, no. SP-2001). Biotinylated secondary antibodies (Perkin Elmer and Dako) and ABC Kit Vectastain Elite (Vector, PK6100) were applied for signal amplifications. Stainings were visualized using DAB substrate (DAKO and Vector Laboratories). Incubation times with DAB substrate were equal for all samples within one staining. Primary antibodies used: α-Lysozyme (Dako, F0372), α-cleaved Caspase-3 (Cell Signaling, 9661), α-CD45 (BioScience, 14-0451), cleaved Caspase-8 (Cell Signaling, 8592), α-ASC (Santa Cruz, #sc-22514-R).

Intestinal epithelial cell isolation

Colon and small intestine were harvested from mice and washed in Ca^{2+} free PBS (Gibco, 14190-094) to remove feces. Tissues were cut longitudinally and incubated in pre-heated 1mM DTT in Ca^{2+} free PBS for 10 minutes at 37°C while shaking. Afterwards, the supernatant was removed, tissues washed in Ca^{2+} free PBS and incubated in pre-heated 1.5mM EDTA in Ca^{2+} free PBS for 15 minutes at 37°C while shacking. Then, tissues were vortexed for 1 minute (small intestine) or 2 minutes (colon) to disconnect IECs from connective tissue. Excessive tissue was removed and the IEC-containing solution centrifuged at 350 x g for 5 minutes at RT. Supernatant was discarded and IEC pellet frozen at -80C or lysed in high salt RIPA buffer.

Protein lysate preparation

Cells (primary and immortalized) were lysed in high-salt RIPA buffer (HEPES (pH7.6) 20nM, NaCl 350mM, MgCl$_2$ 1mM, EDTA 0.5mM, EGTA 0.1mM, Glycerol 20% (v/v), 1% Nonident P-40) on ice for 30 minutes. Cell suspension was centrifuged at 16.000g for 5-20 minutes and supernatant was collected. Protein concentration was measured using PIERCE 660nm Protein Assay Reagent (Thermo Scientific, #22660) and a BSA standard ranging from 0-15 μg/μl. Lysates were adjusted to 2 μg/μl. SDS Lemmli loading buffer (1x final, 1mM DTT, 4% ß-Mecaptoethanol) was added and samples were boiled at 95°C for 5 minutes.

Western blot analysis
Protein lysates were separated by SDS-PAGE and transferred to PDVF-membranes (IPVH00010, Millipore) at 20V for 18h at 4°C or 200mA for 3h at 4°C. Protein size ladder (Thermo Scientific, #26620) was used for size comparison. Membranes were blocked with 5% milk in PBST 0.1% for 1h. Membranes were washed three times with PBST 0.1% for 10 minutes. Membranes were incubated in PBST 0.1% containing primary antibodies O/N at 4°C or RT depending on the primary antibody. Primary antibody species specific secondary antibodies conjugated with horseradish peroxidase were used for detection in combination with chemiluminescent detection substrate (GE Healthcare, RPN2132). Membranes were stripped using stripping buffer (ThermoScientific, 21059) if necessary. Primary antibodies used (m=murine): α-mFADD (Millipore, 05-486), α-mMLKL (Millipore, MABC604), α-mRIPK1 (BD Biosciences, 610459), α-mRIPK3 (Enzo LifeSciences, ADI-905-242-100), α-mGAPDH (Novus Biologicals, (NB300-221), α-mACTIN (SantaCruz, #sc-1616), α-mASC (Adipogen, #AG-25B-0006), α-CRE (Novagen, #69050-3), α-mCaspase-8 (Alexis, ALX-804-447), α-mZBP1 (Adipogen, #AG-20B-0010), α-GSDMD (Abcam, #ab219800), α-phosphorylated-RIPK1 (XXX), α-phosphorylated MLKL (XXX), α-TUBULIN (Sigma, #T6074). Secondary HRP-coupled antibodies (GE Healthcare, Jackson Immuno Research) and chemiluminescent detection substrate (GE Healthcare) were used.
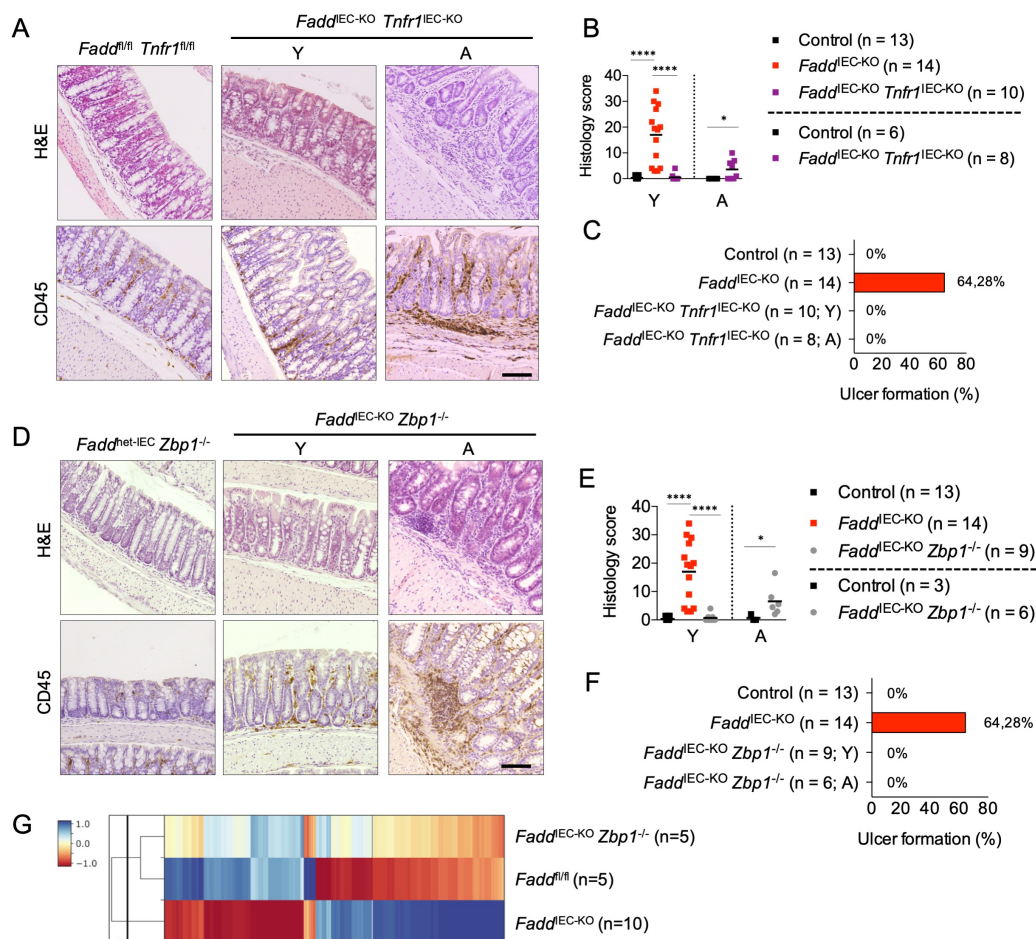
Statistical analysis

Statistical analysis was performed with Prism6, GraphPad. In case of Gaussian Distribution (tested for using D'Agostino-Pearson omnibus normality test), Student's t test was performed. In case of unequal variance, Welch's correction was applied. For non-Gaussian Distribution, Mann-Whitney test was applied. *$p \leq 0.05$; **$p \leq 0.01$; ***$p \leq 0.005$; ****$p \leq 0.001$ for all figures. No data were excluded.

Supplemental Information

Document S1. Figures S1-S5 and Table S1-S2.
Table S2. List of the genotypes and the numbers of mice for which histological sections were analysed for each experimental group. Related to Figures 1, 2, 3, 4, 5, 6, 7, S1, S2, S3, S4 and S5.

Figure 1. Epithelial FADD or caspase-8 deficiencies cause spontaneous colitis

(A) Representative images of colon sections from mice with the indicated genotypes stained with hematoxylin & eosin (H&E) or immunostained for CD45. $Fadd^{fl/fl}$ x $Vil1$-cre ($Fadd^{IEC-KO}$), $Casp8^{fl/fl}$ x $Vil1$-cre ($Casp8^{IEC-KO}$). Scale bar = 100μm.

(B) Histological colitis scores for mice of the indicated genotypes. Each dot represents one mouse. Bars represent mean. **p< 0.01, ***p<0.005, ****p<0.0001.

(C) Percentage of mice with ulcers.

(D) Cluster heat map showing average expression of genes that were significantly changed (fold change ≥ ±1.5, p<0.05) in $Fadd^{IEC-KO}$ and/or $Casp8^{IEC-KO}$ colon tissue compared to floxed control mice. Z-scores are shown.

(E and F) Cluster heat map of gene expression data of selected inflammatory genes in $Casp8^{IEC-KO}$ **(E)** and $Fadd^{IEC-KO}$ **(F)** colon tissue. Z-scores are shown. Each column represents one mouse.

All data from 10-12 week-old mice. Histological images shown are representative of the groups of mice analyzed as indicated in Table S2. See also Figure S1.

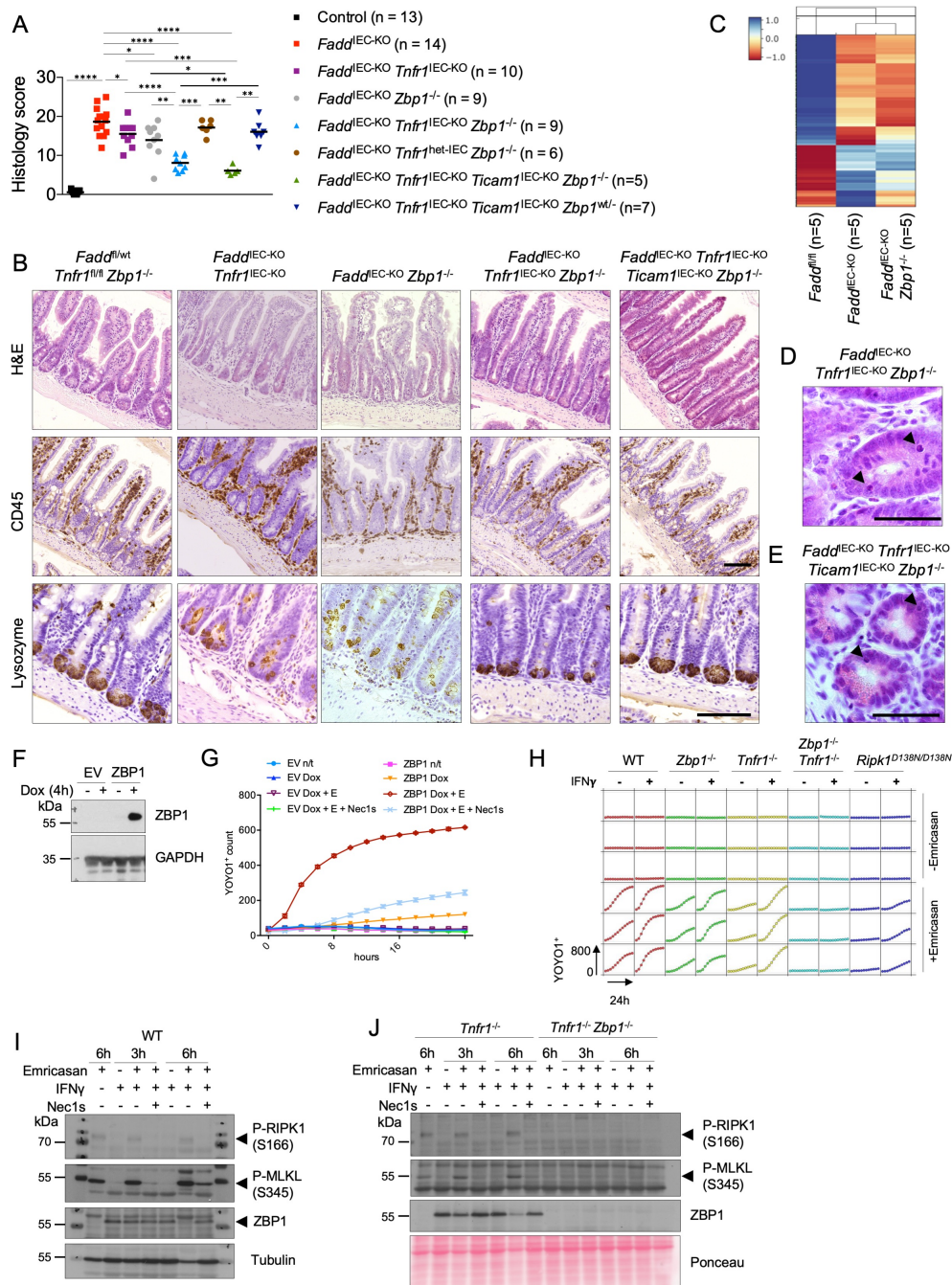**Figure 2. TNFR1 and ZBP1 induce colitis in *Fadd*[IEC-KO] mice**

(A, B and C) Representative images of colon sections stained with H&E or immunostained for CD45 **(A)** and graphs showing histology scores **(B)** and percentage of mice with ulcers **(C)** from young (10-12 week-old, Y) and aged (28-46 week-old, A) mice with the indicated genotypes.

(D, E and F) Representative images of colon sections stained with H&E or immunostained for CD45 **(D)** and graphs with histology scores **(E)** and percentage of mice with ulcers **(F)** from young (10-12 week-old, Y) and aged (36-39 week-old, A) mice with the indicated genotypes.

(G) Cluster heat map showing average expression of genes that were significantly upregulated (fold change ≥ ±1.5, p-value <0.05) in *Fadd*[IEC-KO] colon tissue for the indicated genotypes. Z-scores are shown.

Scale bars = 100μm. Each dot represents one mouse. Bars represent mean. *p<0.05, ****p<0.0001. Histological images shown are representative of the groups of mice analyzed as indicated in Table S2. See also Figure S2.

Figure 3. Redundant functions of TNFR1 and ZBP1 induce ileitis in *Fadd*^{IEC-KO} mice

(A and B) Histological scores **(A)** and representative images of ileal sections stained with H&E or immunostained for CD45 or lysozyme **(B)** from mice of the indicated genotypes. Each dot represents one mouse. Bars represent mean. Scale bar = 100μm.

(C) Cluster heat map showing average expression of genes that were significantly upregulated (cut-off: fold change ≥ ±1.5, p-value <0.05) in the ileum of *Fadd*^{IEC-KO} mice. Z-scores are shown.

(D and E) Representative images of H&E stained ileal sections from mice with the indicated genotypes. Arrowheads mark dying epithelial cells. Scale bar = 50μm.

(F) Immunoblot analysis with the indicated antibodies of protein extracts from MEFs transfected with empty (EV) or doxycycline (Dox)-inducible ZBP1-expressing vectors.
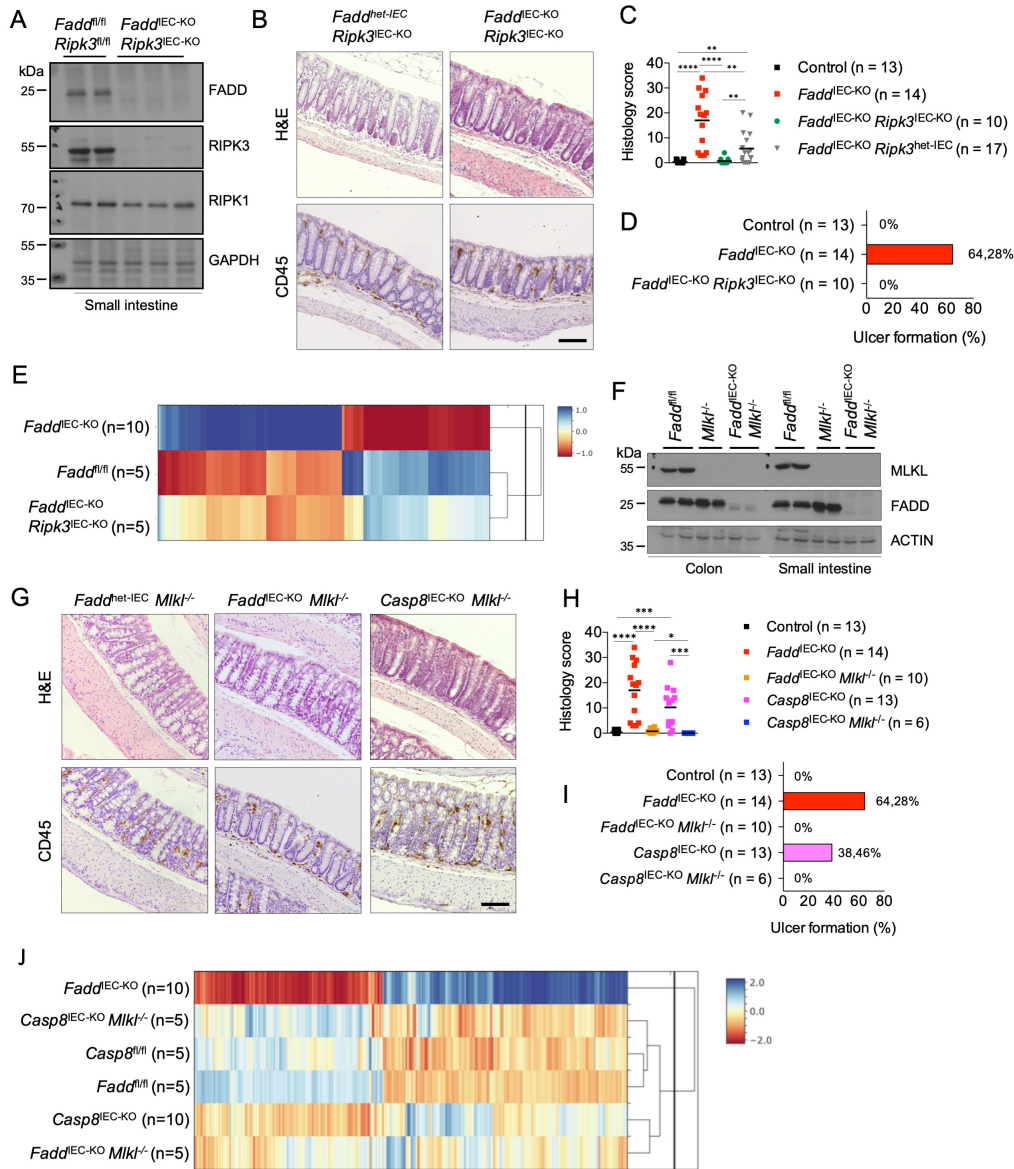
(G) Cell death measured by YOYO-1 uptake in MEFs pretreated with Dox for 24 hours and stimulated with combinations of emricasan (E) and Nec1s. Graph shows mean values from technical triplicates. n/t = no treatment.

(H) Cell death measured by YOYO-1 uptake in primary lung fibroblasts with the indicated genotypes stimulated with IFNγ (24h pre-treatment) and emricasan.

(I and J) Immunoblot analysis with the indicated antibodies of primary lung fibroblasts from WT (I) or *Tnfr1*$^{-/-}$ and *Tnfr1*$^{-/-}$ *Zbp1*$^{-/-}$ (J) mice stimulated with combinations of IFNγ (24h pretreatment), emricasan and Nec1s.

All data from 10-12 week-old mice. Histological images shown are representative of the groups of mice analyzed as indicated in Table S2. Data are representative of three (F-H) or two (I and J) independent experiments.

*p<0.05, **p<0.01, ***p<0.005, ****p<0.0001. See also Figure S3.

Figure 4. MLKL-dependent necroptosis causes colitis in *Fadd*[IEC-KO] and *Casp8*[IEC-KO] mice

(A and F) Immunoblot analysis of IEC protein extracts from mice of the indicated genotypes with the indicated antibodies. Each lane represents one mouse.
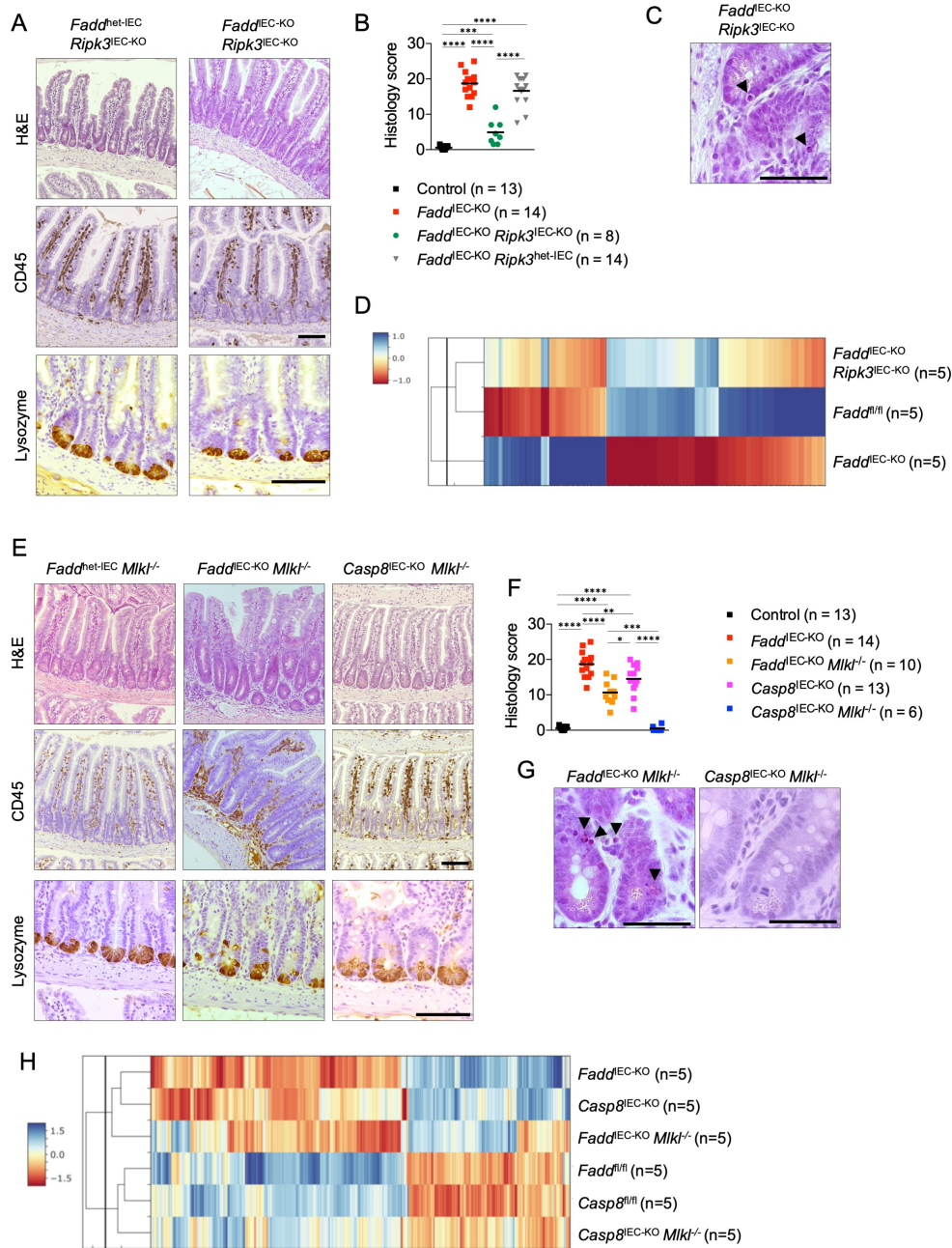
(B, C and D) Representative images of colon sections stained with H&E or immunostained for CD45 **(B)** and graphs showing histology scores **(C)** and percentage of mice with ulcers **(D)** from mice with the indicated genotypes. Scale bar = 100μm. Bars represent mean.

(E) Cluster heat map showing average expression of genes that were significantly upregulated (cut-off: fold change ≥ ±1.5, p-value <0.05) in the colon of *Fadd*[IEC-KO] and/or *Casp8*[IEC-KO] mice. Z-scores are shown.

(G, H and I) Representative images of colon sections stained with H&E or immunostained for CD45 **(G)** and graphs showing histology scores **(H)** and percentage of mice with ulcers **(I)** from mice with the indicated genotypes. Scale bar = 100μm. Bars represent mean.

(J) Cluster heat map showing average expression of genes that were significantly upregulated (cut-off: fold change ≥ ±1.5, p-value <0.05) in colons of *Fadd*[IEC-KO] and/or *Casp8*[IEC-KO] colon tissue. Z-scores are shown.

*p<0.05, **p<0.01 ***p<0.005, ****p<0.0001.

Histological images shown are representative of the groups of mice analyzed as indicated in Table S2. All data from 10-12 week old mice.

Figure 5. MLKL dependent and -independent mechanisms drive ileitis in *Fadd*^IEC-KO mice

(A and E) Representative images of ileal sections from mice with the indicated genotypes stained with H&E or immunostained for CD45 or lysozyme. Scale bar = 100μm.

(B and F) Histological ileitis scores for mice of the indicated genotypes. Each dot represents one mouse. Bars represent mean.
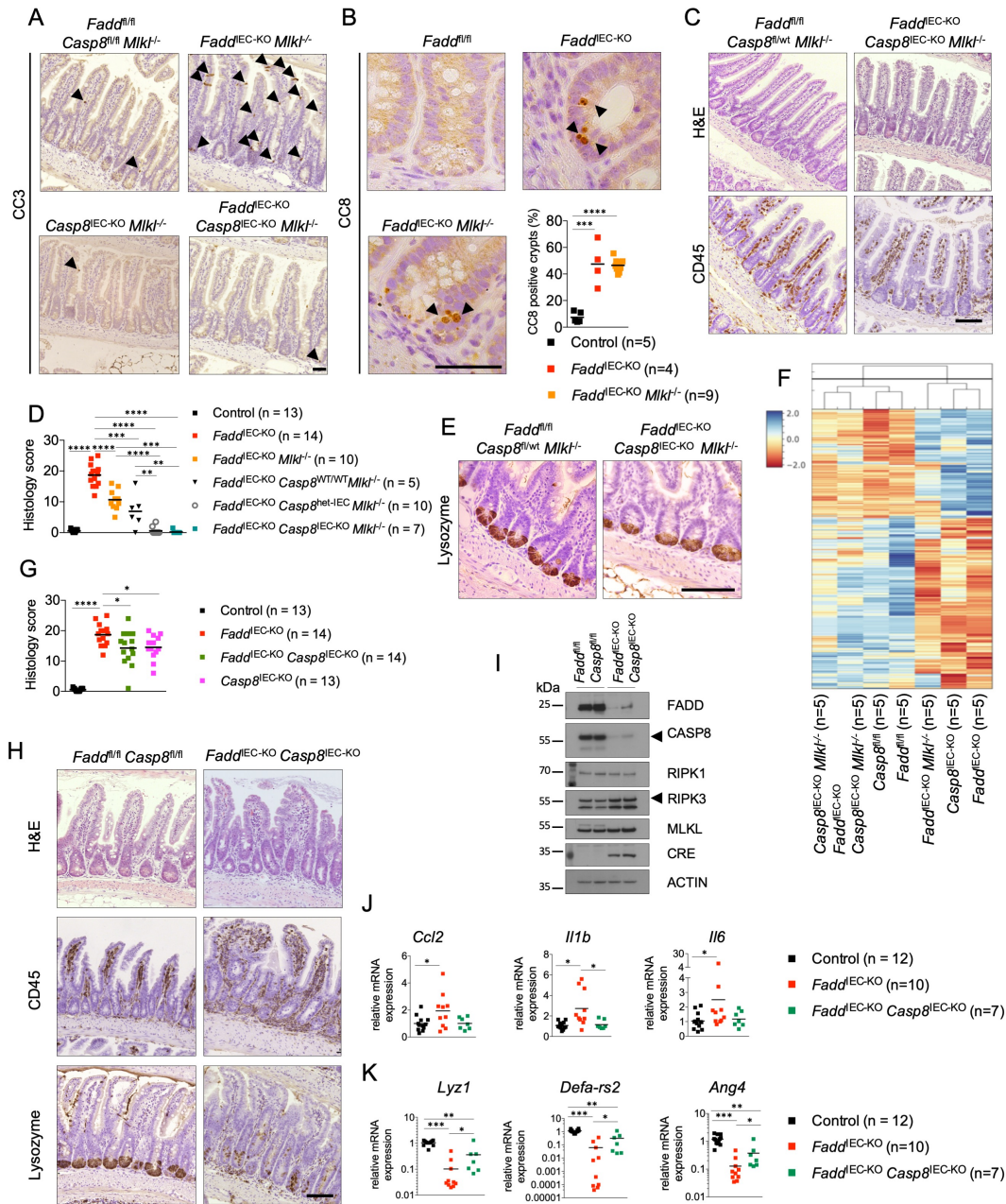
(C and G) Representative images of H&E stained ileal sections of mice with the indicated genotypes. Arrowheads mark dying epithelial cells. Scale bar = 50μm.

(D) Cluster heat map showing average expression of genes that were significantly upregulated (cut-off: fold change ≥ ±1.5, p-value <0.05) in the ileum of *Fadd*^IEC-KO mice. Z-scores are shown.

(H) Cluster heat map showing average expression of genes that were significantly upregulated (cut-off: fold change ≥ ±1.5, p-value <0.05) in the ileum of *Fadd*^IEC-KO and/or *Casp8*^IEC-KO mice. Z-scores are shown.

*p<0.05, **p<0.01, ***p<0.005, ****p<0.0001.

Histological images shown are representative of the groups of mice analyzed as indicated in Table S2. All data from 10-12 week-old mice.

Figure 6. Caspase-8 promotes MLKL-independent ileitis in *Fadd*^{IEC-KO} mice

(A and B) Representative images of ileal sections from mice with the indicated genotypes immonostained for cleaved caspase-3 (CC3) **(A)** or cleaved caspase-8 (CC8) **(B).** Scale bar = 50μm. Graph in **(B)** shows the percentage of ileal crypts with CC8$^+$ cells in mice with the indicated genotypes. Each dot represents one mouse.

(C) Representative images of ileal sections from mice with the indicated genotypes stained with H&E or immunostained for CD45. Scale bar = 100μm.

(D and G) Graphs showing histological ileitis scores in mice of the indicated genotypes. Each dot represents one mouse. Bars represent mean.

(E) Representative images of ileal sections from mice with the indicated genotypes immunostained for lysozyme. Scale bar = 100μm.

(F) Cluster heat map showing average expression of genes that were significantly upregulated (cut-off: fold change ≥ ±1.5, p-value <0.05) in the ileum of *Fadd*^{IEC-KO} and/or *Casp8*^{IEC-KO} mice. Z-scores are shown.

(H) Representative images of ileal sections from mice with the indicated genotypes stained with H&E or immunostained for CD45 or lysozyme. Scale bar = 100μm.
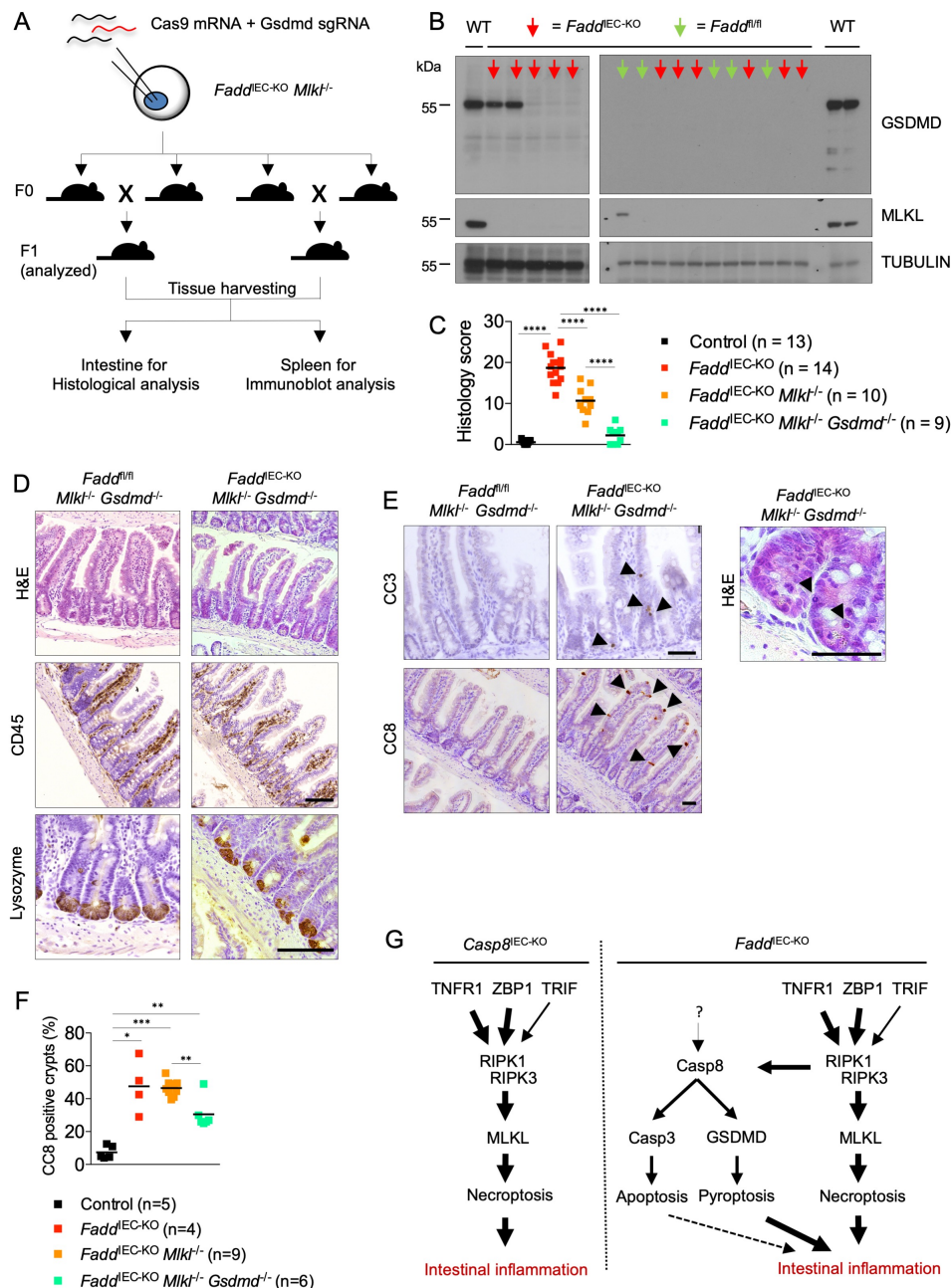
(I) Immunoblot analysis of IEC protein extracts from mice with the indicated genotypes with the indicated antibodies. Each lane represents one mouse.

(J+K) mRNA expression of the indicated genes in the ileum of mice with the indicated genotypes.

*p<0.05, **p<0.01, ***p<0.005, ****p<0.0001.

Histological images shown are representative of the groups of mice analyzed as indicated in Table S2. All data from 10-12 week old mice. See also Figure S4 and Figure S5.

Figure 7. GSDMD mediates MLKL-independent ileitis in *Fadd*[IEC-KO] mice

(A) Strategy for generating and analyzing *Fadd*[IEC-KO] *Mlkl*^{-/-} *Gsdmd*^{-/-} mice.

(B) Immunoblot analysis of spleen protein extracts from F1 mice from (A) with the indicated antibodies. Each lane represents one mouse.

(C) Histological ileitis scores from mice of the indicated genotypes. Each dot represents one mouse. Bars represent mean.

(D) Representative images of ileal sections from mice with the indicated genotypes stained with H&E or immunostained for CD45 or lysozyme. Scale bar = 100μm.

(E) Representative images of ileal sections from mice with the indicated genotypes stained with H&E or immunostained for CC3 or CC8. Scale bar = 50μm. Arrowheads indicate dying epithelial cells (H&E) or CC3 or CC8 positive cells.

(F) Graph showing the percentage of ileal crypts with CC8+ cells in mice with the indicated genotypes. Each dot represents one mouse.

(G) Schematic model depicting the pathways contributing to small intestinal inflammation upon IEC-specific ablation of caspase-8 or FADD.

 *p<0.05, **p<0.01, ***p<0.005, ****p<0.0001. Histological images shown are representative of the groups of mice analyzed as indicated in Table S2. All data from 10-12 week-old mice.